Charles University

Faculty of Science

Study programme: Medicinal Chemistry

Branch of study: Medicinal Chemistry

Monika Spurná

Synthesis of acridone and imidazole-based compounds for potential applications

Syntéza sloučenin na bázi akridonu a imidazolu pro potenciální aplikace

Bachelor's thesis

Supervisor: Dr. Lukáš Rýček, M.Sc.

Praha, 2025

Prohlášení

Prohlašuji, že jsem závěrečnou práci zpracovala samostatně a že jsem uvedla všechny použité informační zdroje a literaturu. Tato práce ani její podstatná část nebyla předložena k získání jiného nebo stejného akademického titulu.

V Praze, 15.05.2025

Podpis

Abstrakt

Tato bakalářská práce představuje syntézu a fluorescenční intenzitu modulující vlastnosti imidazol-akridonových derivátů. Mezi klíčové reakce v jejich syntéze patřila Ullmannova kondenzace následovaná cyklizací, tvorba imidazolu pomoci Debus-Radziszewského reakce a N-alkylace. Syntetizovaný imidazol-akridon a jeho alkylovaná sůl byly zkoumány z hlediska jejich fluorescenčního chování za různých podmínek pH. Alkylovaná sůl byla dále podrobena zkoumání změny intenzity fluorescence na základě přítomnosti různých kovových iontů. Výsledky potvrzují funkčnost těchto sloučenin jako fluorescenčních sond a sloučeniny budou dále studovány pro pH detekci a jako molekulární switche pro ukládání dat na molekulární úrovni.

Klíčová slova: deriváty akridonů, imidazol-akridon, fluorescenční sondy, pH detekce, detekce kovových iontů, molecular switch, molecular data storage

Abstract

This bachelor thesis presents the synthesis and fluorescence intensity-modulating properties of imidazole–acridone derivatives. The key reactions in synthesis included Ullmann condensation with subsequent cyclisation, Debus–Radziszewski imidazole formation, and N-alkylation. Synthesized imidazole acridone and its alkylated salt were investigated for their fluorescence behaviour under various pH conditions. Additionally, the alkylated salt underwent study of change in fluorescence intensity based on the presence of various metal ions. The results confirm their functionality as fluorescent probes, and the compounds will be further studied for pH sensing and as molecular switches for molecular data storage.

Key words: acridone derivates, imidazole-acridones, fluorescent probes, pH sensing, metal ion sensing, molecular switches, molecular data storage

Table of contents

Used acronyms and abbreviations

acac – Acetylacetonate

ADOHcy – S-Adenosylhomocysteine

ADOMet – S-adenosylmethionine

AMP – Adenosine monophosphate

at – apparent triplet

ATP – Adenosine triphosphate

BODIPY – Boron-dipyrromethene

bs – broad singlet

CoA – Coenzyme A

ctDNA – Calf thymus DNA

DCM – Dichloromethane

DMF – Dimethylformamide

DMSO – Dimethyl sulfoxide

DPPH – 2,2-diphenyl-1-picrylhydrazyl

ESI – Electrospray ionization

ESI^+ – Positive electrospray ionization

FRET – Förster resonance energy transfer

G4 – G quadruplex

GFP – Green fluorescent protein

HCMV – Human cytomegalovirus

HIV – Human immunodeficiency virus

HRMS – High-resolution mass spectrometry

hROS – Highly reactive oxygen species

HSV – Herpes simplex virus

ICT – Intramolecular charge transfer

IR – Infrared spectroscopy

Malonyl-CoA – Malonyl coenzyme A

MDR – Multidrug resistance

M.p. – Melting point

MS – Mass spectrometry

n.d. – Not determined

NMR – Nuclear magnetic resonance

PDT – Photodynamic therapy

PET – Photoinduced electron transfer

PP_i – Inorganic pyrophosphate

ROS – Reactive oxygen species

RT – Room temperature

SM – Starting material

SSDs – Solid-state drives

TEA – Triethylamine

TLC – Thin layer chromatography

Ts – Tosyl

UV – Ultraviolet

Vis – Visible

1. Introduction

Acridone is a tricyclic nitrogen-containing heterocycle that has gained interest due to its unique properties. Together with its derivatives, acridone has attracted attention in recent years due to its broad range of biological activities, potential for novel therapeutic use and technical applications. While acridine derivatives were historically more prominent, now the focus of modern research has also turned to acridones, because of their more selective biological pathways. Both acridine and acridone derivates are valuable for their versatile pharmacological properties, that include anti-cancer, anti-inflammatory, anti-bacterial, and anti-malarial effects. The importance of new therapeutic methods is becoming increasingly prevalent in the context of growing antibiotic resistance.[1]

Moreover, these derivates demonstrate potential in areas beyond traditional drug development. Acridones possess strong fluorescence, enabling their use as molecular probes and switches capable of responding to environmental stimuli. Their interactions with metal ions further enhance their biological activity, supporting applications in biosensing and therapeutics.

Combined with acridone, N-heterocyclic carbene-based compounds such as imidazole are of significant interest in medicinal chemistry. This stems from their ability to enhance fluorescence, despite not being innately fluorescent themselves.[2] Their capacity to exist in multiple states, such as protonated or deprotonated, depending on environmental conditions, allows for excellent modulation of fluorescence properties. This adaptability makes them particularly valuable for applications as molecular probes or switches, applicable for sensing specific elements in biological systems, or in optical data storage systems.

In this context, this thesis focuses on the synthesis of imidazole–acridone compounds and the investigation of their fluorescence intensity change based on environmental conditions. These properties are explored while assessing their potential as fluorescent probes and molecular switches for data storage.

2. Theoretical part

2.1. History and structure of acridine and acridone

Acridine and acridone (Scheme 1) are planar, tricyclic heterocycles composed of fused benzene and pyridine rings. They differ at position 9 – acridone features a carbonyl group, classifying it as a ketone, while acridine does not. Both compounds maintain full aromaticity and structural rigidity. Their planar geometry contributes to their stability and reactivity, enhancing their intercalation ability and influencing their many photophysical properties.

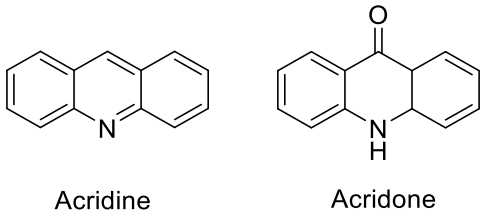

Scheme **1** Structure of acridine and acridone

The beginning of acridone and acridine originates back in the late 19th century. Acridine was first isolated in 1870 by Gräbe and Werner[3], who identified it as a naturally occurring compound in coal tar. In the early 20th century, acridine derivatives became widely used in the dye and pigment industry. They also served as antiseptics and anti-malarial agents during both World Wars, before being superseded by penicillin.[3]

Acridone was mainly researched in 1914 by Karl Drechsler[4], who further advanced its understanding, exploring its structure and synthesis, thus broadening its chemical and medicinal potential. Acridone quickly became a subject of growing interest for its photophysical properties and later for its biological activities.

The melting point of the parent acridone is 354 °C, and it appears as a yellow solid. Despite being insoluble in common solvents like ethanol, water, or chloroform, it dissolves in N,N-dimethylformamide (DMF), dimethyl sulfoxide (DMSO), and alcoholic potassium hydroxide. Acridone's resistance to heat, oxidation, and photodegradation makes it extremely stable and luminous, properties that further contributed to its industrial and scientific applications.[1]

The interest in acridone compounds skyrocketed later in the 20th century, as researchers began to explore their potential in medicinal chemistry. Over the past few decades, research into acridones has advanced significantly. Scientists have also isolated natural acridones from various plant sources, leading to a surge in interest for their use in drug development. [5]

2.2. Typical synthesis of acridone core

Acridine can be synthesized through various methods, such as the Bernthsen synthesis, the Friedländer reaction, and by reduction of acridone.[6] In contrast, acridone has significantly fewer synthetic routes available, which limits the flexibility of its preparation.

2.2.1. Synthesis via N-arylanthranilic acid derivatives

The primary method for acridone synthesis consists of Ulmann condensation and subsequent cyclisation (Scheme 2). First, in Ulmann condensation, copper powder acts as both a catalyst and halogen acceptor from aryl halides. Copper typically provides higher yields compared to copper oxides. The base (K_2CO_3) absorbs the released HX (X = Cl, Br, I), which is essential to promote the reaction. Heating formed N-arylanthranilic acid in concentrated sulfuric acid or polyphosphoric acid induces cyclization that results in acridone.[7,8]

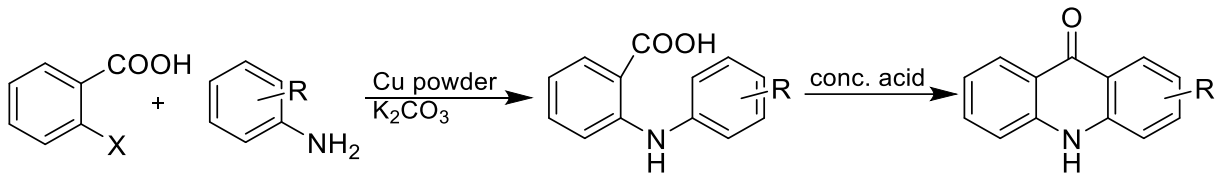

Scheme **2** Acridone synthesis via N-arylanthranilic acid derivatives

2.2.2. Synthesis via benzophenone

The synthesis of acridone derivatives through benzophenone intermediates has been significantly less used than the Ullmann condensation method. First introduced by Lewis, this approach involves base- or heat-driven substitution of alkoxy groups of benzophenone that is usually made using standard Friedel–Crafts reactions. Its limited application stems likely due to regioselectivity challenges.[7]

A variant synthesis (Scheme 3), by Horne and Rodrigo, uses an anionic Fries rearrangement of N-tosyl-*o*-iodobenzanilide to generate a benzophenone intermediate. Next, it undergoes one-step cyclization and fluorine substitution with tetraethylammonium hydroxide (NEt_4OH) resulting in acridone formation.[9]

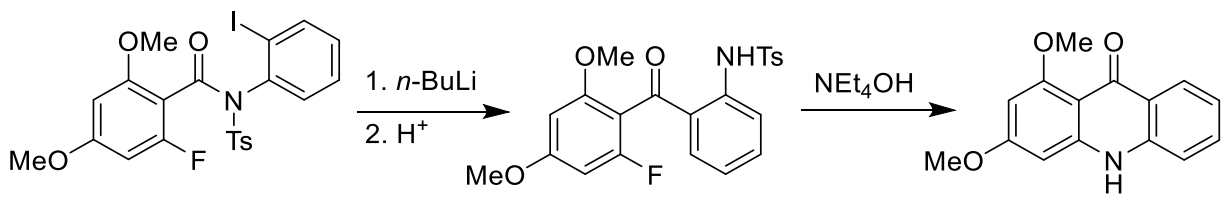

Scheme **3** Synthesis of acridone by Horne and Rodrigo

2.3. Naturally occurring acridone alkaloids

Natural acridones are primarily found in the Rutaceae family[10], known for its aromatic plants, including citrus species and *Ruta graveolens*. These alkaloids, examples of which are shown in (Scheme 4), are recognized for their structural diversity and many biological activities. They demonstrate antifungal, herbicidal, larvicidal, anticancer, and antimalarial activities.[11]

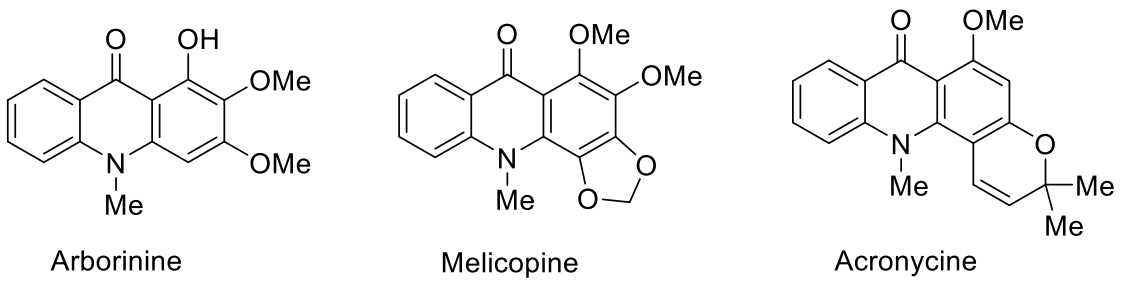

Scheme **4** Structures of some natural alkaloids

Arborinine demonstrates potent anticancer effects against cervical cancer cells. It is capable of inducing apoptosis without causing DNA damage and preventing cancer cell migration by downregulating key regulators of epithelial-mesenchymal transition.[12] Melicopine displayed cytotoxic and antimalarial activities *in vitro*.[13] Similarly, acronycine and its many derivatives are notable for their high antiproliferative activities. They are capable of alkylating guanine sites in DNA, illustrating their prominent anticancer abilities.[14] These substances also demonstrate selective cytotoxicity to cancer cells while preserving normal cells, resulting in fewer adverse effects.[1]

As shown in (Scheme 5), the biosynthesis of acridone alkaloids starts with the methylation of anthranilate to form N-methylanthranilate, which is then activated to N-methylanthraniloyl-CoA, a key substrate. This activated compound condenses with malonyl-CoA, a reaction catalysed by acridone synthase, forming the acridone skeleton. The pathway concludes with cyclization, yielding acridone derivative.[15,16]

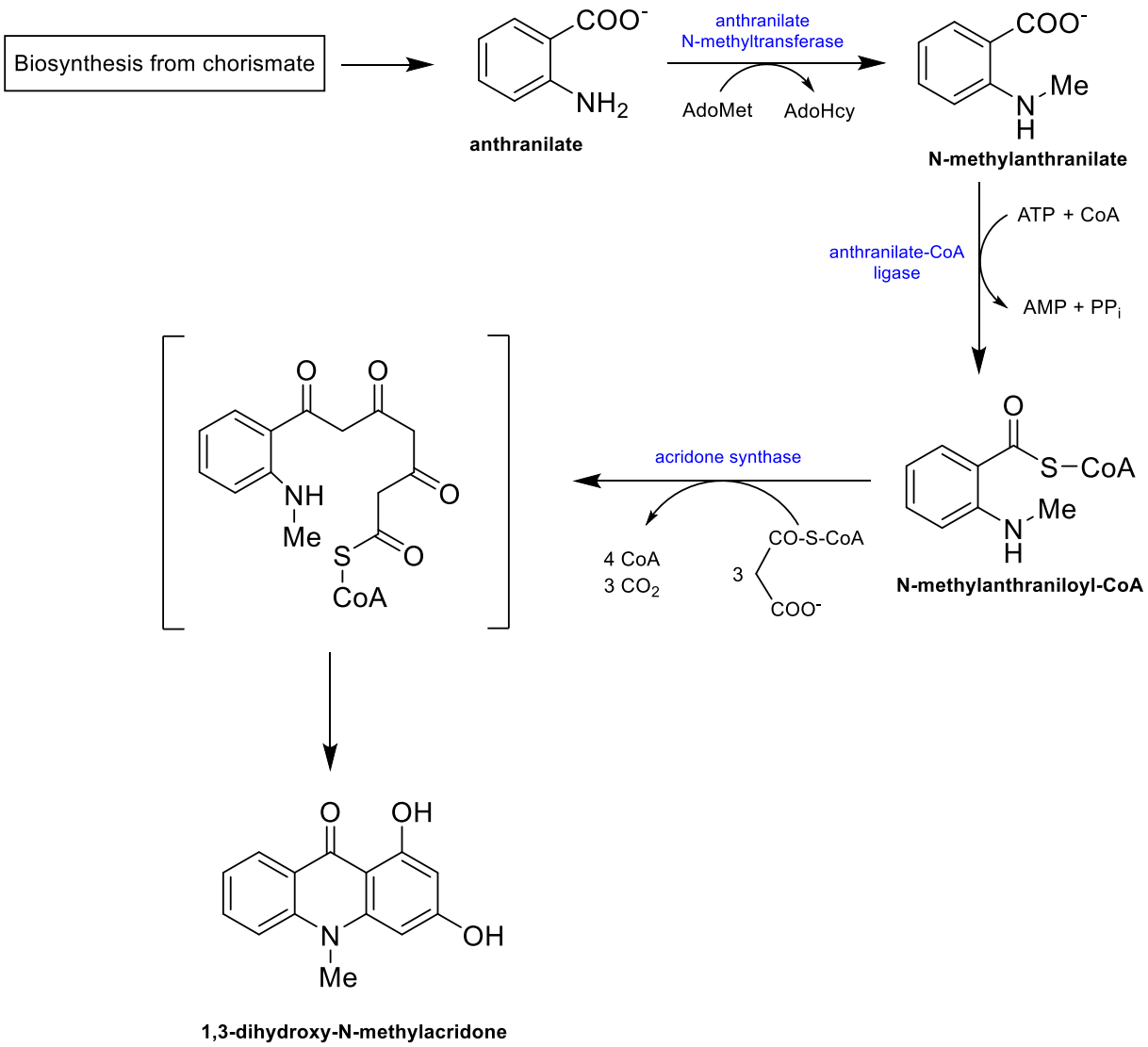

Scheme **5** Acridone alkaloids biosynthesis[16]

2.4. Biological properties

Acridone derivatives have gained considerable attention due to their broad range of biological activities (Figure 1). Compared to their acridine counterparts, acridones exhibit a more targeted approach in biological pathways. Their derivatives show strong antibacterial activity against both gram-positive and gram-negative bacteria, such as *Staphylococcus aureus* and *Escherichia coli*[1], in addition to activity against viruses such as herpes simplex virus (HSV-1 and HSV-2), human immunodeficiency virus (HIV), human cytomegalovirus (HCMV), and others.[7]

Their planar tricyclic aromatic structure allows intercalation into DNA, disrupting essential cellular functions and making them potent candidates as DNA-targeting agents. Moreover, they show potent abilities in inhibiting topoisomerase II, as observed in compounds like acronycine, acronycine epoxide, and benzo[b]acronycine.[1,17] Some derivates, like acridone–pyridine hybrids, stabilize G4 structures at telomeres on DNA. This prevents telomerase from extending telomeres, therefore limiting the uncontrolled proliferation of cancer cells.[18] Other derivatives act as protein kinase inhibitors, targeting for example MARK4 – which suppressed cancer cell proliferation, increased ROS levels and induced apoptosis.[19]

Acridones also combat multidrug resistance (MDR) – a significant challenge in cancer therapy where cancer cells develop resistance to a broad range of chemotherapeutic agents. Acridone derivatives have been shown to overcome MDR by inhibiting P-glycoprotein, a key protein involved in the efflux of drugs from cancer cells.[20] Additionally, several derivatives promise notable antioxidant properties, as shown by effectively scavenging DPPH free radicals *in vitro*.[21]

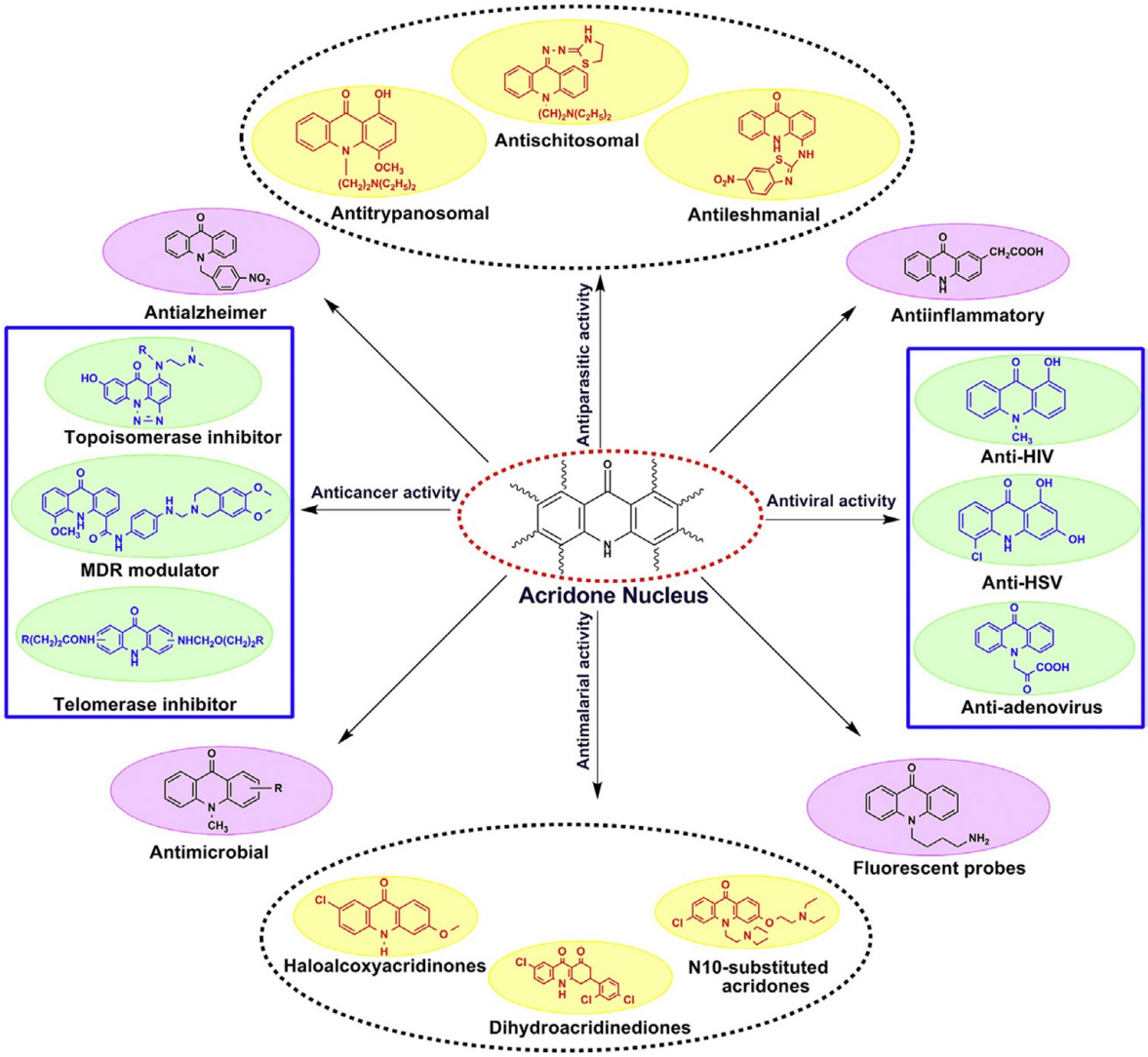

Figure **1** Biological properties of acridone[7]

2.5. Other potential applications

2.5.1. Photodynamic therapy

Acridone derivatives, with their strong fluorescence and ability to generate ROS upon light activation, are promising candidates for photodynamic therapy (PDT). As photosensitive compounds, they enhance PDT's effectiveness in selectively targeting cancer cells. The proposed porphyrin-acridone hybrids are combining PDT with DNA cleavage.[22] Acridine orange (Scheme 6) is considered as an novel photosensitizer for PDT, as it demonstrates low-toxicity effect.[23]

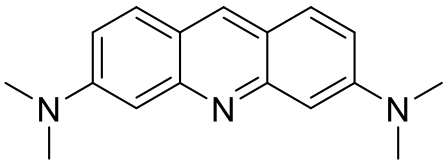

Scheme **6** Acridine orange

2.5.2. Fluorescent probes

Fluorescent probes can be categorized into small-molecule and macromolecular types based on their structure. Macromolecular fluorescent probes typically consist of protein-based fluorophores. A standout example is the green fluorescent protein (GFP), obtained from the jellyfish *Aequorea victoria*. GFP has become a valuable tool for monitoring gene expression and tracking protein localization in living cells and organisms. Additionally, GFP has been optimized and incorporated into various proteins through mutagenesis and protein engineering that resulted in the creation of diverse biosensors, physiological sensors and photochemical data storages.[27]

Fluorescent probes based on small organic molecules have become indispensable tools in modern biology, as they provide dynamic information about the localization and quantity of the molecules of interest. Their major advantage is that they often do not require genetic modification of the sample, unlike protein-based probes, which moreover face the limitations of their large size (>20 kDa) and the need to be typically attached at either the N-terminus or C-terminus, making them unsuitable for labelling internal regions of the protein.[24]

These small-molecule probes respond by altering their fluorescence emission based on specific binding events, chemical reactions, or changes in their local environment. Beyond assessing overall cell viability, fluorescent probes can be designed to detect pH changes, metal ions, reactive oxygen, nitrogen and sulphur species, enzymatic activity and membrane potential. This

makes them highly versatile tools in both fundamental and applied biosciences. They are widely applied in drug discovery, cellular imaging, environmental monitoring, and various clinical diagnostics. Their popularity stems from the high sensitivity of fluorescence detection, the exceptional spatial and temporal resolution offered by fluorescence microscopy, and the commercial availability of a broad range of fluorophores.[25,26]

Small-molecule fluorophores are widely used for their compact size, adjustable photophysical properties, and easy chemical modification. Common types with the description of their optical properties are depicted in Figure 2, and in addition to acridines and acridones, include coumarins, naphthalimides, fluoresceins, rhodamines, BODIPYs and cyanines.[25]

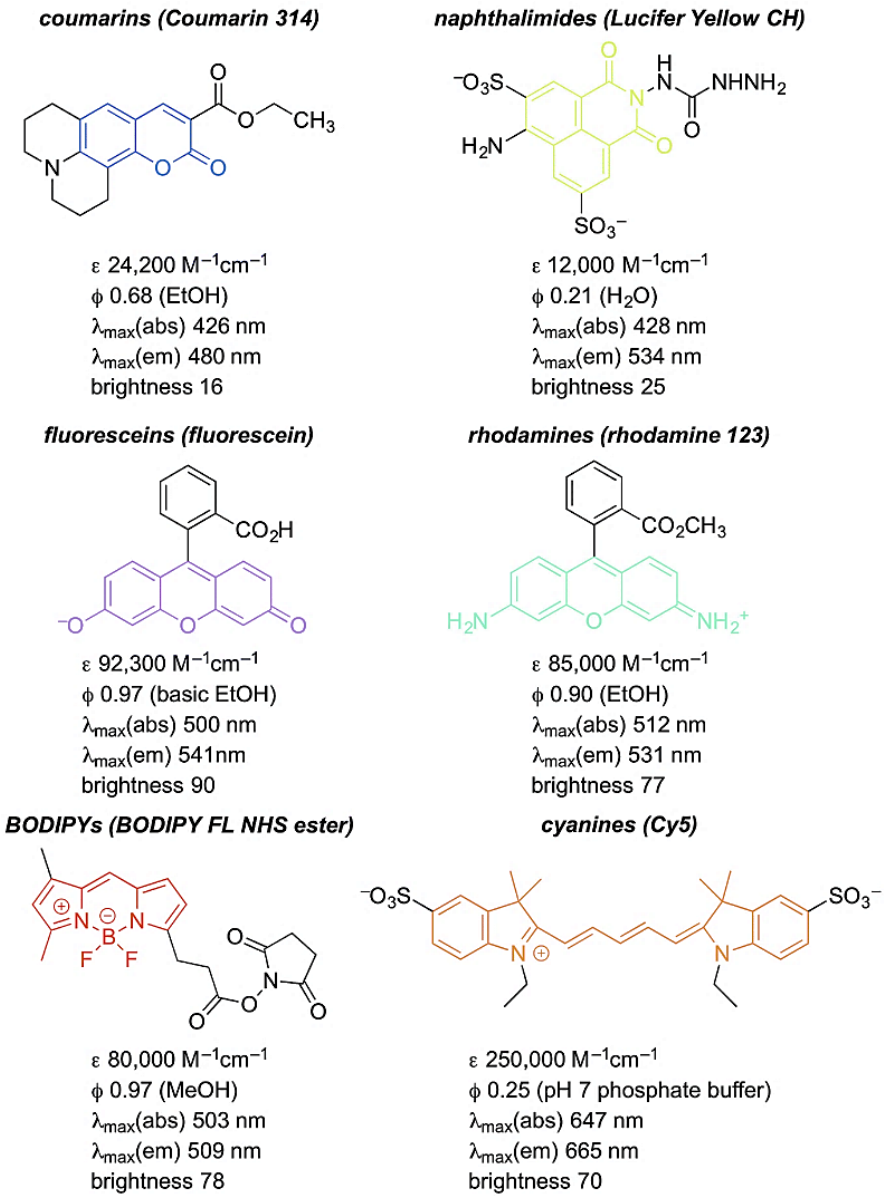

Figure **2** Fluorescent probes of common small-molecule chromophores[25]

Fluorescence in most probes is controlled by three main mechanisms that allow for sensitive responses to environmental or molecular changes: Photoinduced electron transfer (PET), where electron transfer can quench or restore fluorescence; intramolecular charge transfer (ICT), where shifts in electron distribution affect emission; and Förster resonance energy transfer (FRET), where energy is transferred between nearby fluorophores based on distance and spectral overlap.[25]

The probe **A,** with the structure of fluorescein-like fluorophore (Scheme 7), is PET quenched by an electron-rich 4-hydroxyphenyl ether moiety. Upon reaction with specific highly reactive oxygen species (hROS), particularly the ˙OH radical and reactive intermediates of peroxidase and cytochrome P450, the ether is cleaved through O-dearylation. This disrupts PET and restores strong fluorescence of fluorescein core.[28,29]

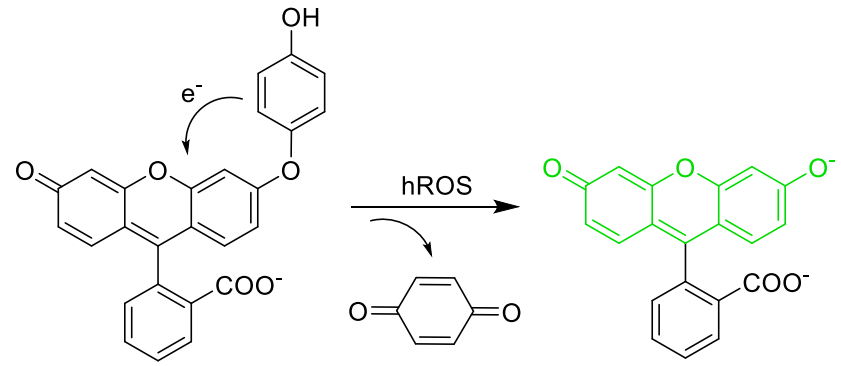

Scheme 7 PET based fluorescent probe

ICT involves an electron donor and acceptor within a fluorophore. Excitation increases dipole moment, causing solvent relaxation and red-shifted emission. ICT strength affects emission wavelength—enhanced ICT leads to longer wavelengths, while reduced ICT causes blue shifts. External stimuli like metal binding or chemical reactions can modulate ICT, altering fluorescence. An H_2S responsive probe **B** using a BODIPY fluorophore (Scheme 8) has initially quenched fluorescence due to strong ICT between the donor and an aldehyde acceptor. Reaction with H_2S removes the aldehyde, eliminating ICT and restoring fluorescence.[25,30]

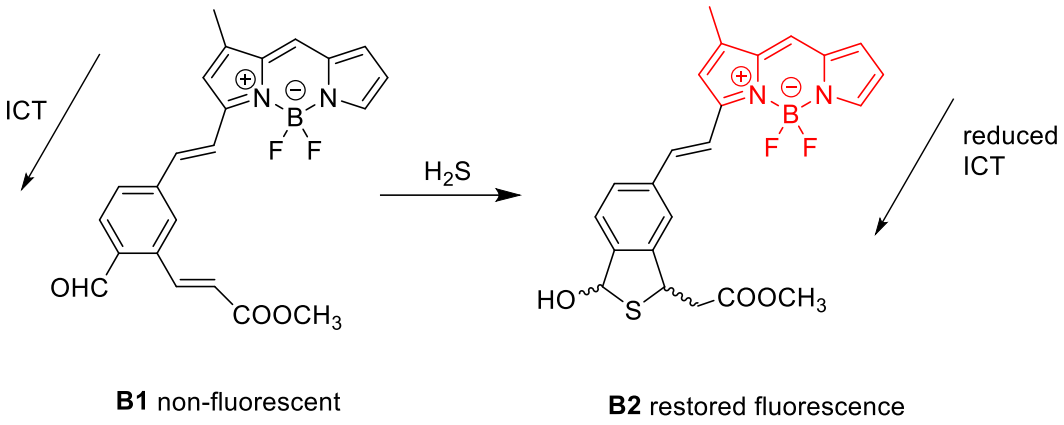

Scheme **8** ICT based fluorescent probe

The probe **C** in Scheme 9 functions as a FRET-based fluorescent pH sensor combining a coumarin donor and a rhodamine acceptor. With decreasing pH, fluorescence shifts from blue to red due to enhanced FRET efficiency as rhodamine becomes emissive. It operates effectively in the pH range of 4.20–6.00, demonstrates low cytotoxicity and good photostability in HeLa cells, and selectively stains lysosomes.[31]

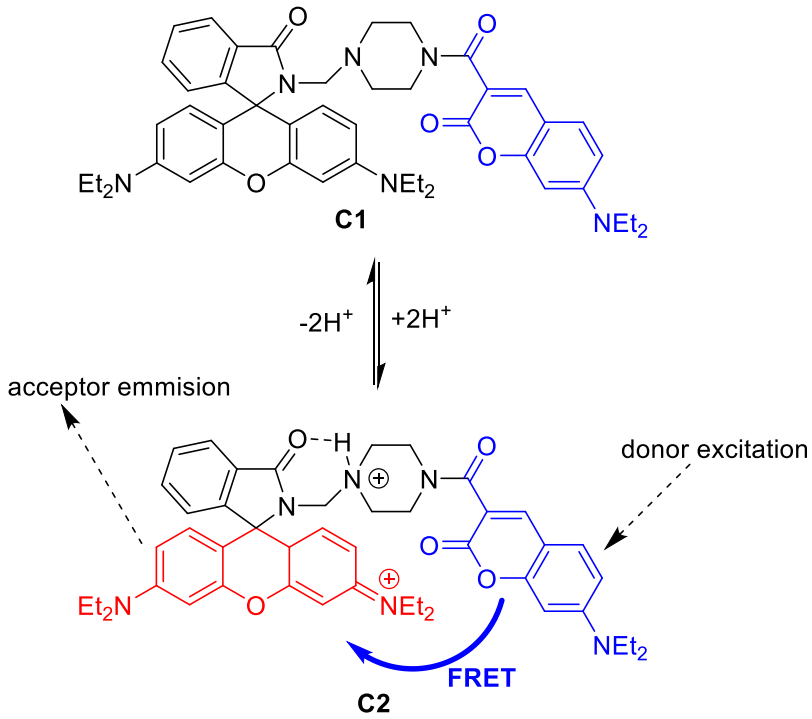

Scheme **9** FRET based fluorescent probe

2.5.2.1. Acridone fluorescent probes

Acridone and its derivatives are highly effective fluorescent probes because their rigid, planar π-conjugated structure allows efficient light absorption and strong fluorescence emission. The possible combination of electron-donating and electron-accepting groups enhances charge transfer within the molecule, improving fluorescence quantum yield and stability. Modifications at different positions on the acridone ring can fine-tune their optical properties allowing the development of tailored fluorescent sensors. Among their positives also stands long fluorescence lifetimes, large Stokes shifts, and excellent photostability, which reduce background noise and prevent photobleaching. Additionally, their small size supports easy cell penetration and low toxicity, making them ideal for biological imaging and sensing applications.[32]

Acridones are used in biological research for their fluorescent properties that enable a wide range of applications. Some acridone derivatives have been shown to bind selectively to DNA, enabling their use as nuclear stains in live/dead cell discrimination and in fluorescence-activated cell sorting for cell cycle analysis. Additionally, their ability to selectively bind biomolecules has led to the development of acridone-based sensors for pH, metal ions, and specific molecules, such as nitric oxide or ATP. Overall, acridones have established themselves a flexible structure for designing multifunctional sensors suited to a wide range of cellular and biochemical studies.[7]

DNA-tagging acridone probes (Scheme 10)

Probe **D** combines a pharmacophore pterocarpan with an acridone fluorophore. It binds to the DNA's minor grove activating fluorescence and enabling DNA detection.[33] Probe **E**, is a small-molecule fluorescent probe used to detect calf thymus DNA (ctDNA). **E** binds to DNA and exhibits a linear fluorescence response with varying DNA concentrations, making it suitable for quantitative DNA analysis. ctDNA is purified DNA source extracted from the thymus gland of young calves and is commonly worked with for its availability and well-characterized sequence.[34]

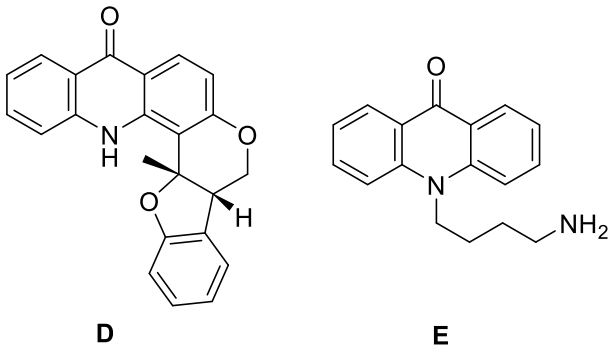

D E

Scheme **10** Structures of DNA probes **D** and **E**

Acridone probes for monitoring metabolism and signalling pathways (Scheme 11)

ATP-selective acridone-based probe, **F**, was developed to monitor enzymatic reactions, enabling the study of metabolic processes related to ATP generation and consumption.[35] The fluorescent probe **G** effectively senses nitric oxide with a fluorescence increase. It is capable of detecting nitric oxide in living Jurkat cells.[36]

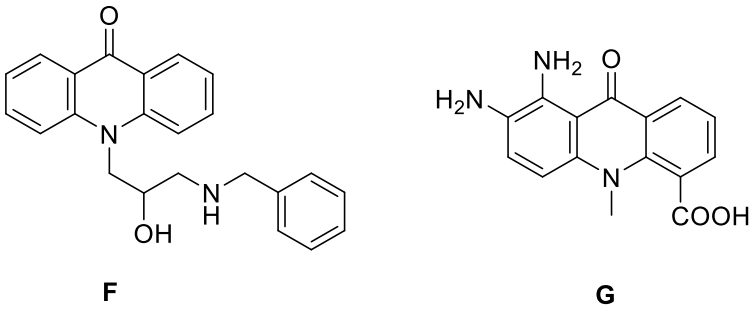

F G

Scheme **11** Structures of probes **F** and **G**

pH based acridone probes (Scheme 12)

Acridone derivatives are highly sensitive to environmental factors like pH changes. The fluorescence of acridone can be strongly influenced by the protonation or deprotonation on added functional groups – such as amines, carboxyls, or hydroxyls.

It was demonstrated that acridones pH probes can be tailored for specific environments. Some, like compound **H**, function only in acidic conditions, while others, such as compound **I**, are effective across a broader pH range. It was observed that structural features like fluorine substitution enhance their fluorescence behaviour in both acidic and basic environments. [37]

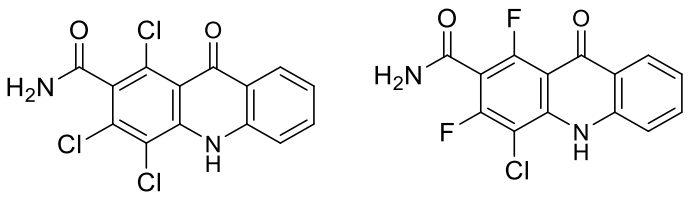

H **I**

Scheme **12** Structures of pH probes **G** and **H**

Metal ion sensing acridone probes (Scheme 13)

Acridone–imidazole hybrids show promise in metal ion sensing due to their nitrogen and oxygen donor atoms, which enable metal coordination, and their stable fluorescent core. Upon binding metal ions, these probes often exhibit measurable changes in fluorescence – either quenching or enhancement – depending on the ion type. A key factor in designing effective sensors is selectivity, as a as clear differentiation between ions is essential for practical use. Although this area remains relatively underexplored, both acridone derivatives without imidazole and imidazole-based systems combined with other fluorophores have demonstrated metal-sensing capabilities, highlighting the broader potential of these structures in sensor development.

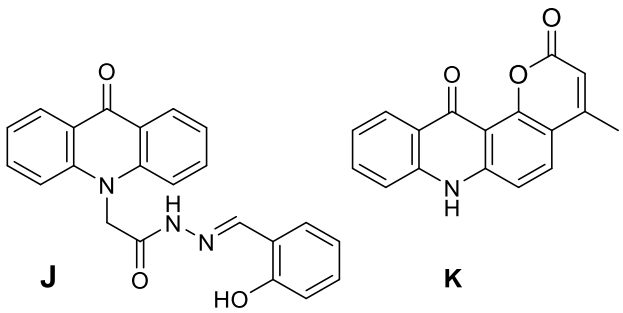

J **K**

Scheme **13** Structures of metal ion selective fluorescent probes **J** and **K**

In the study reported by M. Aarjane, an N-acylhydrazone acridone derivate **J** was shown to be highly sensitive and selective for copper ions in aqueous media. A clear response to Cu^{2+} was demonstrated, all the while other metal ions produced no significant effect. Figure 3 shows a graph of all tested chloride salts, displaying a clear selectivity for Cu^{2+} ions.[38]

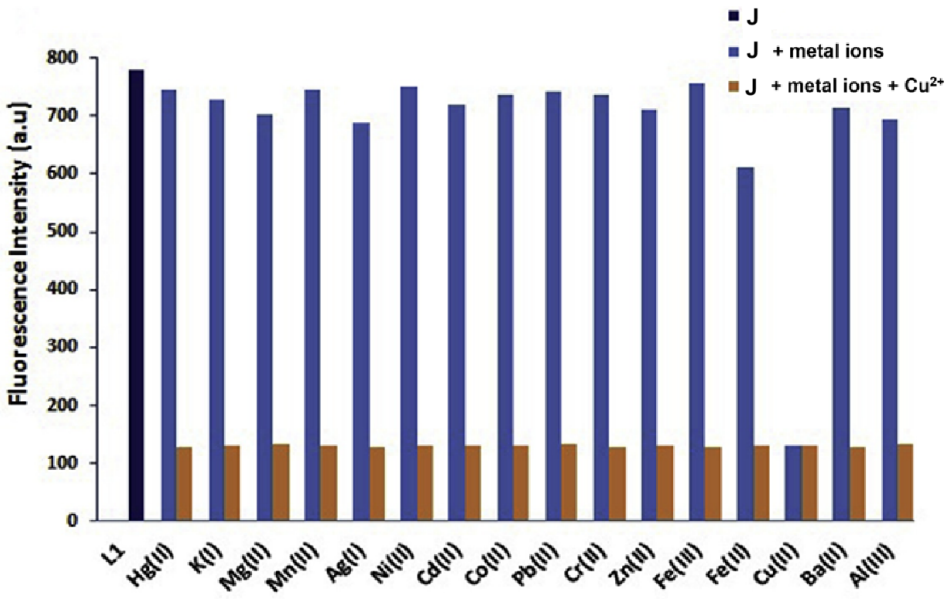

Figure **3** Comparison of fluorescence intensity change of **J** due to presence of various metal cations

Next, the coumarin–acridone fluorescent probe **K**, reported by Jiayong Huang, has already proven to be effective in cellular and *in vivo* imaging. It demonstrated high selectivity and sensitivity for Fe^{3+}. The presence of Fe^{3+} effectively quenched the fluorescence of the probe, allowing for clear detection. It showed a linear fluorescence response and maintained strong stability under physiological conditions, with minimal interference from other metal ions. Figure 4 shows images of HeLa cells and zebrafish incubated with probe **K** along with various concentrations of Fe^{3+}.[39]

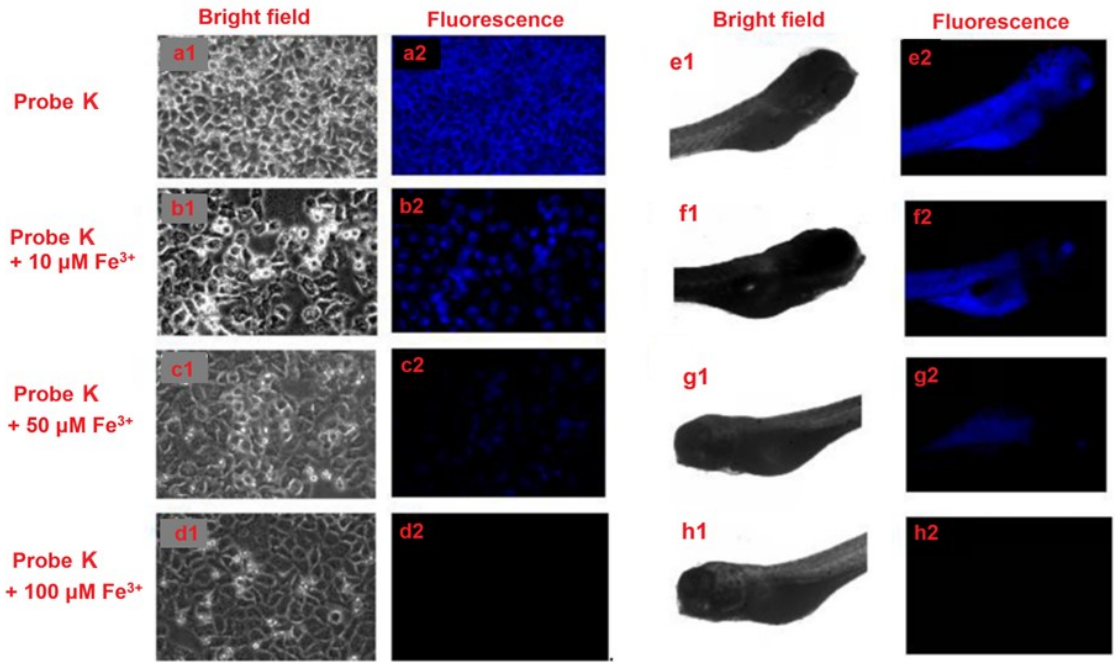

Figure **4** Bright field and fluorescence images of HeLa cells incubated with probe **K** (10.0 μM) (a1, a2) and further incubated with addition of Fe^{3+} (b1, b2, c1, c2, d1, d2); bright-field and fluorescent images of zebrafish incubated with probe **K** (10.0 μM) (e1, e2), further incubated with addition of Fe^{3+} (f1, f2, g1, g2, h1, h2)

2.5.3. Molecular switches

While fluorescent probes are designed to emit light in response to specific targets or environments, molecular switches go a step further by responding reversibly to specific stimulus. These systems can shift between states when exposed to stimuli such as pH shifts, metal ions, light, electric fields, temperature changes, redox processes, or chemical modifications. This alters their fluorescence response. A light-based molecular switch with fulgide structure and dual photoreactive 1,3,5-hexatriene moiety is shown in Scheme 14. The structures commonly employed for molecular switching besides fulgides include diarylethenes, spiropyrans, azobenzenes, DNA/RNA-based switches, and redox-active species such as ferrocene.[40]

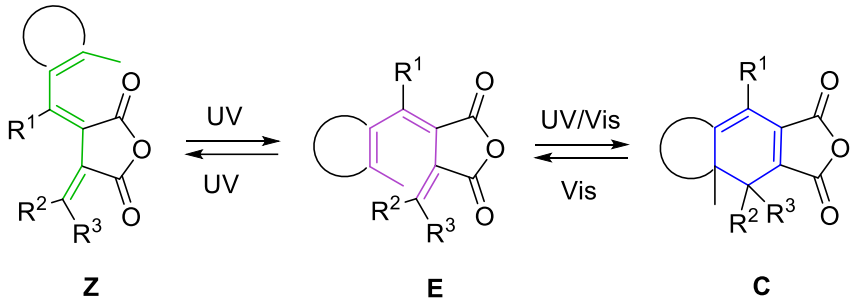

Scheme **14** Fulgide-like optical molecular switch[41]

Molecular switches offer innovative dynamic control that makes them invaluable for real-time sensing, logic operations, and molecular memory devices. Additionally, they shows promise in gene therapy, cellular signalling, modulating protein function, while working as biosensors and diagnostics agents.[42,43]

2.5.3.1. Molecular data storage systems

Molecular switches are promising in molecular data storage systems since they can switch states reversibly, making them ideal for encoding rewritable information. With the exponentially growing volume of data being generated globally, traditional silicon-based systems are constrained by storage density, energy usage, and lifetime. Silicon systems like SSDs suffer from limitations like storage capacity, repeated rewrites, and loss of data on removal from a power supply. This has led the way to explore non-silicon systems that have the capability to provide more capacity, longer duration, and better energy efficiency. Devices to store data on a molecular scale use switches that encode information as a binary bit using stable molecular states as a "0" and a "1". These molecules are modulated between the states by external cues, including pH, light, or electrochemical conditions, as illustrated in

Scheme 15. Switches based on imidazoles, capable of reversibly existing in many states, find particular utility.

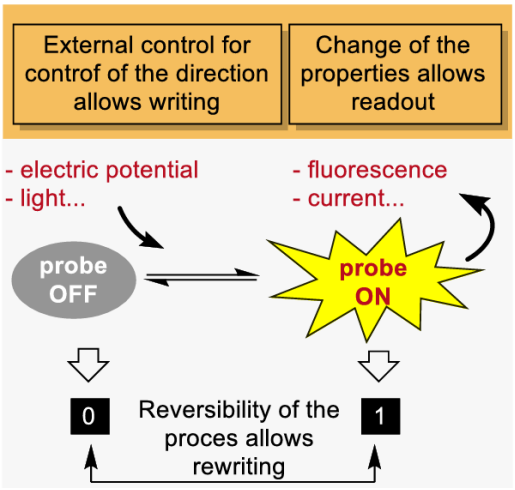

Scheme **15** Basic principle of molecular data storage

3. Goals

The main goals of this work are:

1. The synthesis of imidazole-acridone **3** and alkylated imidazolium salt **4** (Scheme 16)
2. Testing of their fluorescence intensity modulating properties in various acid-base forms
3. Testing of suitable compounds' selective fluorescence properties in the presence of various metals

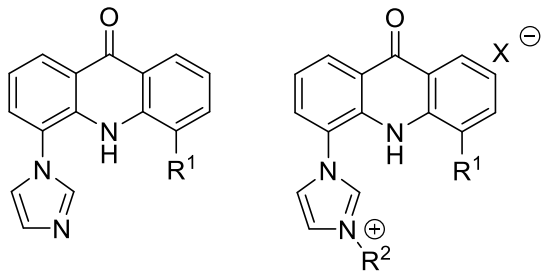

3 **4**

Scheme **16** Structure of imidazole-acridone **3** and alkylated imidazolium salt **4**

4. Results and discussion

According to the retrosynthetic analysis (Scheme 17), the target imidazolium **4** will be disconnected at the N-alkyl bond, showing that the final step is a simple N-alkylation using an appropriate alkyl halide. The imidazole ring in **3** is formed through Debus–Radziszewski synthesis[44], a cyclocondensation reaction using a carbonyl compound and an ammonium source. The acridone core in **2** is accessible through an intramolecular cyclisation reaction. The acridone precursor **1** can be synthesized via an Ullmann-type coupling reaction[7], in which an *ortho*-halobenzoic acid **SM1** reacts with aminobenzene derivative **SM2** under copper catalysis.

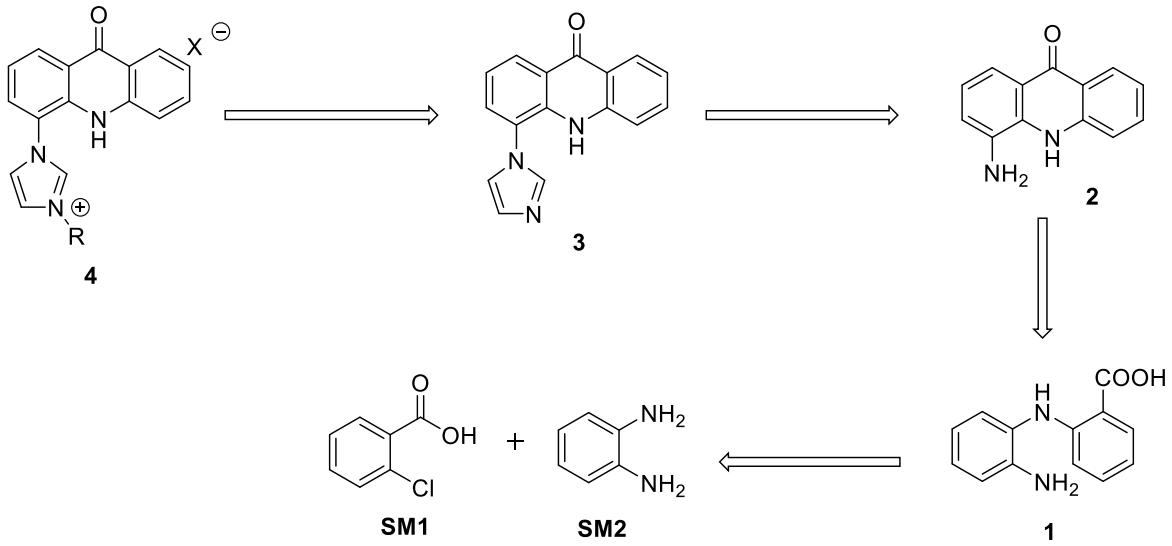

Scheme **17** Retrosynthetic analysis

4.1. Ullmann condensation

Compound **1** was synthesised using *ortho*-chlorobenzoic **SM1** acid and *ortho*-phenylendiamine **SM2**. Copper powder was used as a catalyst and potassium carbonate as a base. The reaction was carried out in DMF under reflux and an inert atmosphere for 16 hours (Scheme 18).

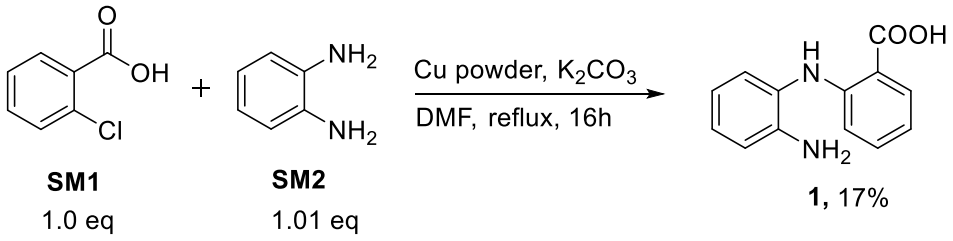

Scheme **18** Synthesis of **1**

Isolation of the compound posed a major problem. Attempts to replicate the protocol reported by Lin Tian[45] were unsuccessful. As per the instructions, the crude reaction mixture was treated with acid in water; however, the product, which is capable of forming a zwitterion, did not precipitate as expected. Extraction proved unsuitable, as the product exhibited similar distribution between the organic and aqueous phases. An attempt to crystalize the compound was made; nevertheless, the process in acetonitrile, ethanol, and isopropanol failed.

The central problem was the difficulty of removing DMF, as it could not be easily evaporated on a rotavap. Other solvents, such as MeCN were considered for the reaction; however, DMF was necessary due to the required high temperature. In the end, it was decided that the most straightforward way was to remove DMF from the reaction mixture by vacuum distillation.

Subsequently, the crude product was subjected to column chromatography with DCM/MeOH as a mobile phase. Nonetheless, due to the compound's tendency to remain trapped in the column and the presence of various side products with similar R_f values, a second round of column chromatography was required. Eventually, we were able to obtain the desired compound, albeit in 17% yield.

4.2. Cyclisation and formation of acridone core

Aminoacridone **2** was prepared by intramolecular electrophilic aromatic substitution of compound **1** in excess polyphosphoric acid while stirring and heating the mixture to 120 °C for 2.5 hours (Scheme 19).

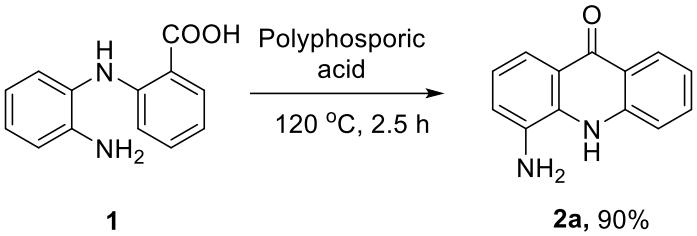

1 **2a**, 90%

Scheme **19** Synthesis of **2a**

After the reaction, the mixture was diluted in water and neutralized with 6 M KOH solution, while being cooled in an ice bath, leading to the precipitation of the product. However, inconsistently, two spots may have been observed on the TLC. The cause of this was unclear, as the NMR spectrum of the product was pure. These spots were too close to each other, therefore could not be separated by column chromatography. It was later concluded that, during the neutralization process monitored using pH paper, various acid-base forms of the product were formed (Scheme 20). In hindsight, the reaction proceeded smoothly, with yields reaching up to 90%.

The ^{1}H NMR spectra of different forms of **2a** (Figure 5) were obtained by adding to an NMR tube containing neutral product a drop of 1 M aqueous HCl solution for acidic form and a drop of 2 M aqueous NaOH solution for basic form. The middle spectrum (in green) depicts the neutral form where we can see both the enaminone NH proton (the most downfield signal) and the amine group NH_2 (the most upfield signal). The top spectrum (in blue) displays the deprotonated form, which lacks acidic enaminone NH proton. In the bottom spectrum (in red) of the protonated form we see an overall shift downfield due to increased acidity. The most downfield signal represents enaminone NH proton. NH_3^+ is not observed most likely due to its rapid proton exchange.

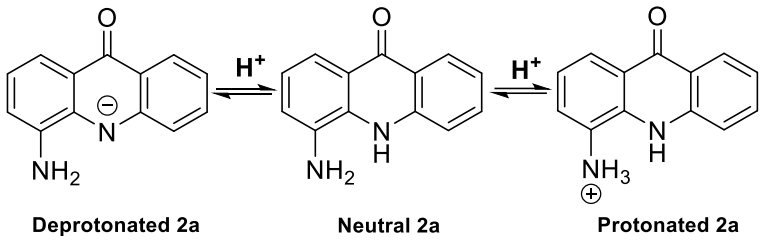

Scheme **20** Acid-base forms of **2a**

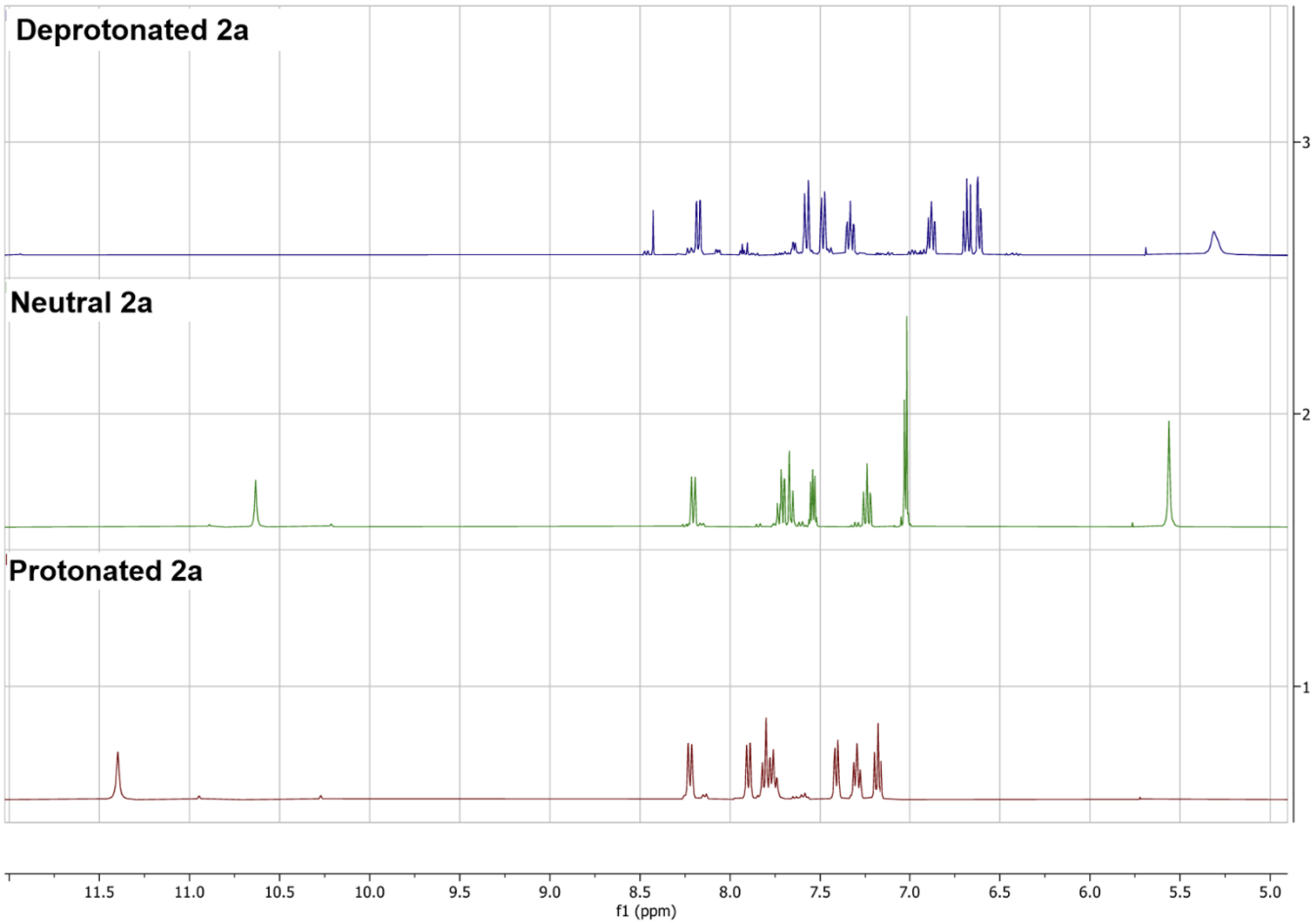

Figure **5** NMR of various acid-base forms of **2a**

4.3. Debus-Radziszewski's formation of imidazole ring and acid-base properties

4.3.1. Synthesis

Compounds **3a** and **3b** underwent synthesis via the Debus–Radziszewski reaction. The transformation consists of three steps: 1.) condensation of the amine with glyoxal, 2.) condensation with ammonia, generated from ammonium salt, and formaldehyde, and 3.) dehydration with phosphoric acid. The reaction was carried out in MeOH (Scheme 21).

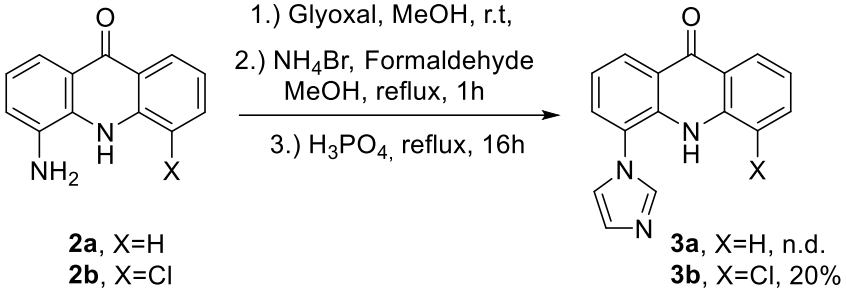

Scheme **21** Synthesis of **3a** and **3b**

Originally, solely compound **2a** was intended for this reaction. The reaction was not proceeding as expected, so the quality of the reactants was investigated. ^{1}H NMR analysis revealed that both glyoxal and formaldehyde were impure, likely due to oxidation. Consequently, a fresh bottle of glyoxal was used, and formaldehyde was replaced with paraformaldehyde to lessen toxicity. However, due to the low yield of the initial Ullmann condensation used to obtain the starting amine **2a**, there was not enough material to proceed efficiently nor confirm formation of compound **3a**. Therefore, the strategy was changed to use compound **2b**, which was commercially available.

The acridone core **2b** was treated with glyoxal (1.2 eq) in MeOH. This reaction could not be monitored using neither TLC nor ^{1}H NMR. The ^{1}H NMR spectrum showed only broad peaks, suggesting presence of intermediates, making it impossible to interpret the data. Various reaction times were tested, initially 4 hours, but later extended to overnight to achieve a slightly higher final yield.

The second step involved an addition of paraformaldehyde (2 eq) and ammonium bromide (2 eq), followed by refluxing for one hour, and lastly, step three consisted of dehydration reaction triggered by an addition of H_3PO_4, and overnight reflux. An attempt was made to add TEA (2 eq) during the second step to better promote the generation of ammonia from NH_4Br.

Despite the logical reasoning behind this, the result was an increased formation of side products and a lower yield.

The work-up for the involved filtering the solids from the crude mixture, which were assumed to be inorganic. However, the NMR analysis suggested that these could be also unspecific fragments of the acridone core. Afterwards, the solvent was evaporated from the filtrate, and the mixture was neutralized in water with strong base which caused precipitation of the product. The neutralization process, which was controlled with pH papers, resulted in the formation of various acid-base forms of imidazole-acridone **3b** (Scheme 22), similarly to acridone **2a.**

The crude precipitate was then collected by vacuum filtration. Although extraction of the product from the aqueous phase with EtOAc was attempted, the product obtained was impure, and the amount was inconsequential. Furthermore, the product showed limited solubility in most solvents, including DMSO, which complicated its characterization.

The major side-product was a highly polar impurity, that analysis of which was complicated by the low solubility both in water and in the organic solvents. Column chromatography was used to isolate the pure product, albeit in various acid-base forms. In the end, the highest yield that was achieved in this reaction was 20%. This is in line with some literature sources, which indicate that this reaction typically yields low results and produces mixtures of by-products, including reversed aldol condensations and oxazole formations[46] while also suffering from a higher energy barrier.[47]

4.3.2. Acid-base and optical properties

The ^{1}H NMR spectra of different forms of **3b** (Figure 6) were obtained by adding to an NMR tube containing neutral product a drop of 1 M aqueous NaOH solution for basic form and subsequently, a drop of 2 M aqueous HCl solution for acidic form. The middle spectrum (in green) depicts the neutral form where we can see the enaminone NH proton (the most downfield signal). The top spectrum (in blue) displays the deprotonated form, which lacks the enaminone NH signal, consistent with the loss of one proton. The remaining signals are more spread out, with shift both upfield and downfield, indicating that the loss of proton has altered the molecule's charge distribution. In the bottom spectrum (in red) of the protonated form we see an overall shift downfield due to increased acidity. The most downfield signal represents enaminone NH proton. These states proved reversible, as after basifying the solution again, the spectrum returned to the deprotonated form, and subsequent acidification regenerated the protonated form.

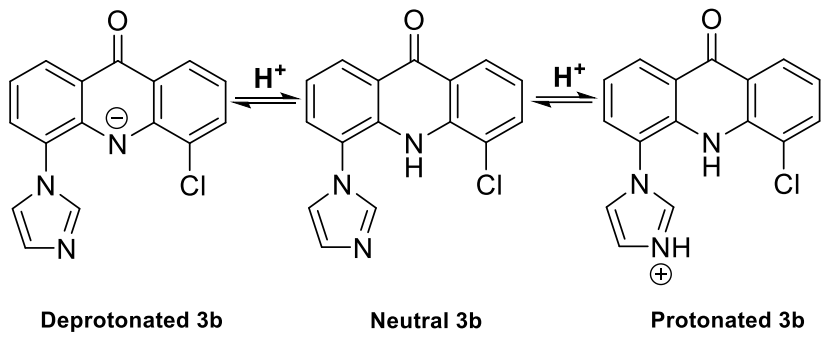

Scheme **22** Acid-base forms of **3b**

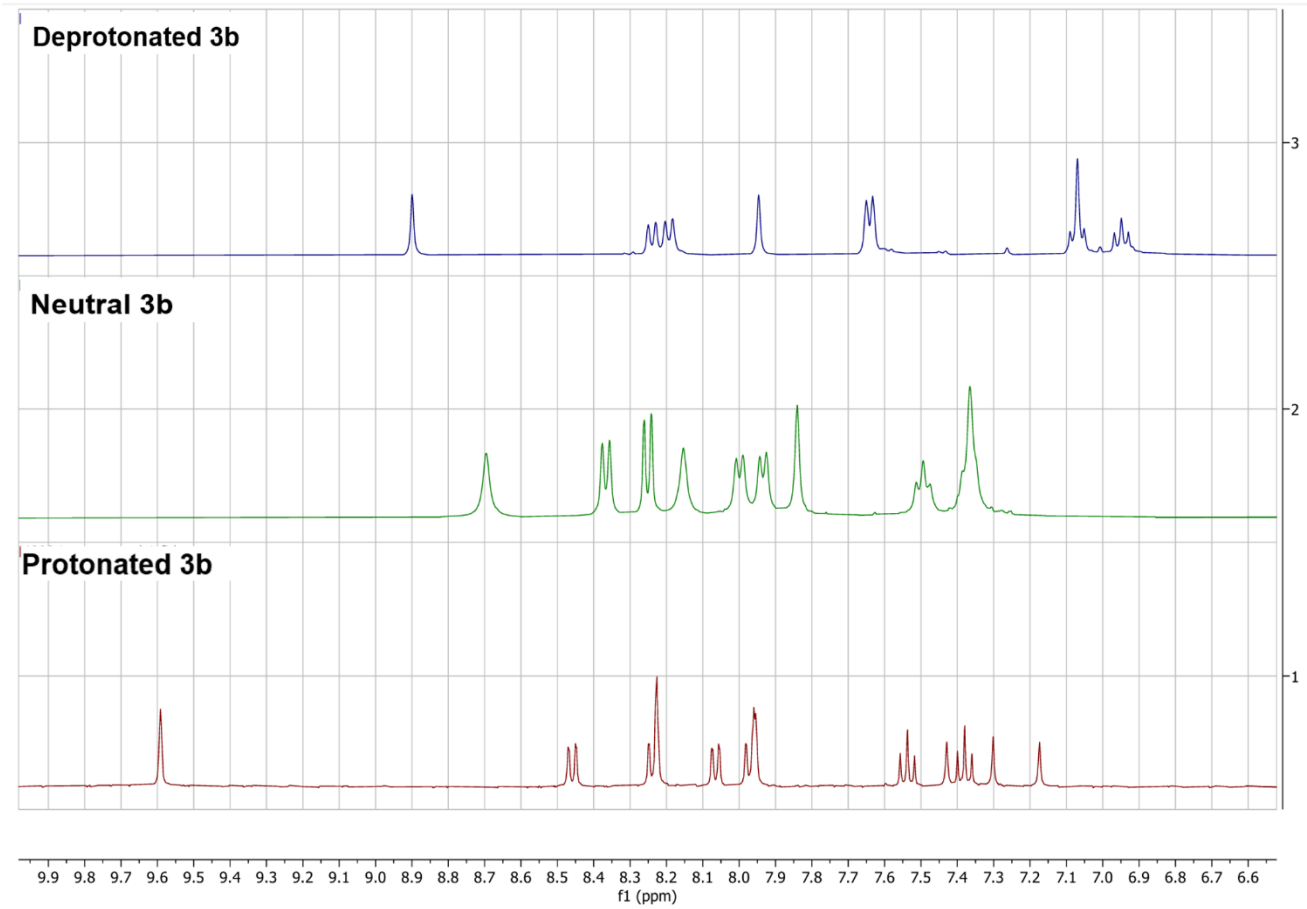

Figure **6** NMR of various acid-base forms of **3b**

The UV-Vis spectra of all forms of **3b** were measured (Figures 7–9). It was observed that protonated and neutral form exhibit distinct absorption maxima at 389.33 nm and 388.05 nm, respectively. The deprotonated form exhibited weaker band at 343.3 nm along with extra peaks at 403.36, 428.70, and 452.82 nm. These measured wavelengths provided us a solid basis to proceed with fluorescence measurements using available transilluminator longwave UV light (365 nm). It was expected, that at this wavelength, the protonated and neutral form should exhibit fluorescence, while the lower absorption of the basic form would lead to the decrease

of the fluorescence. Such system would be suitable for pH dependent fluorescent switch, with possible application in reversible data storing, or a pH probe for possible monitoring of pH in living systems.

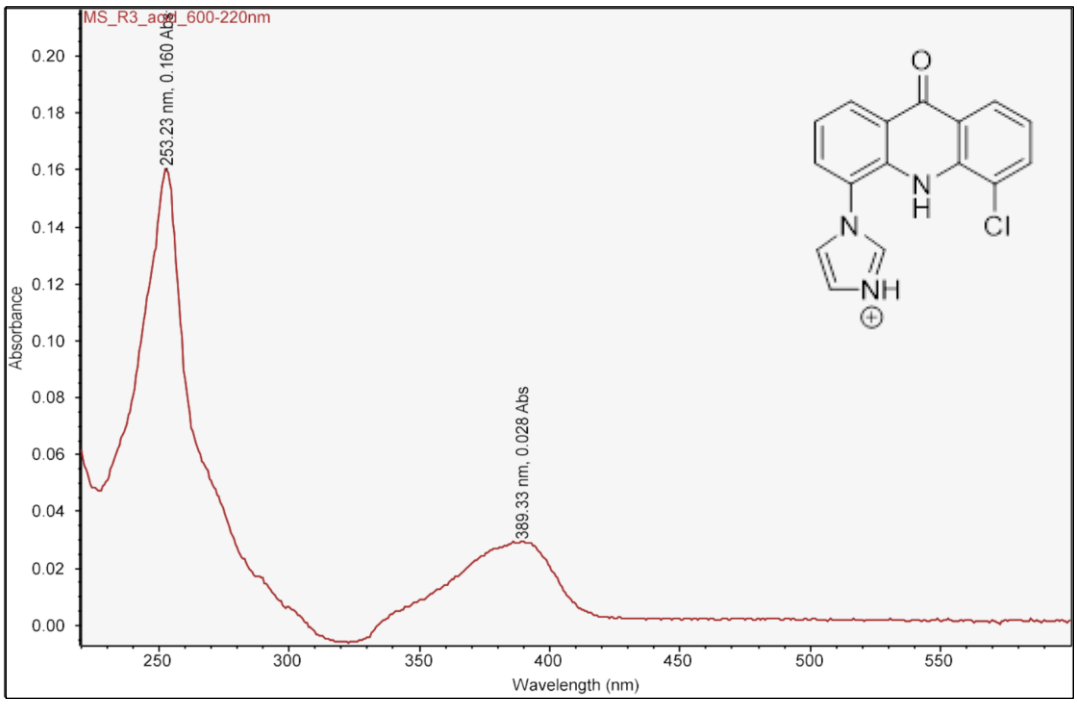

Figure **7** UV-Vis absorption spectrum of **protonated 3b**

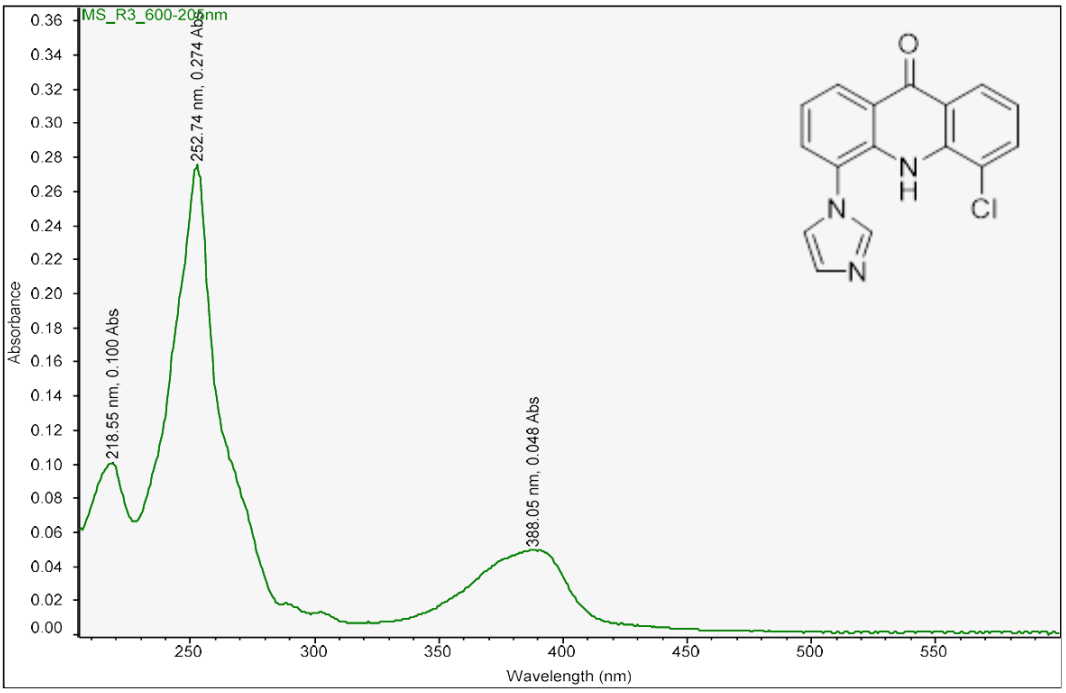

Figure **8** UV-Vis absorption spectrum of **neutral 3b**

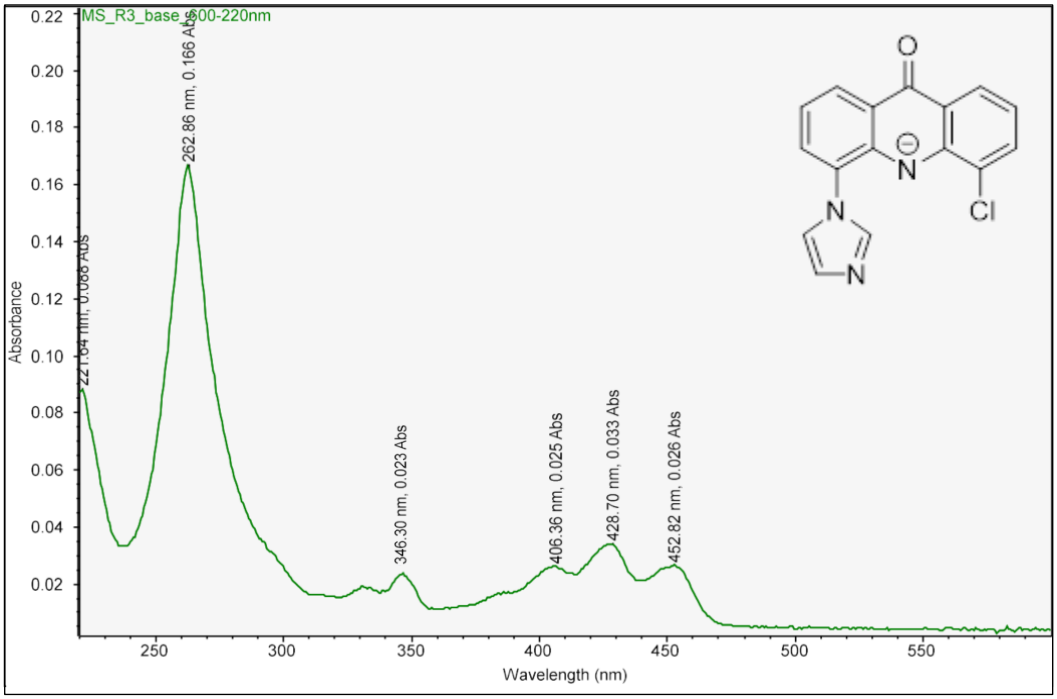

Figure **9** UV-Vis absorption spectrum of **deprotonated 3b**

To measure the fluorescence intensity, a 365 nm longwave transilluminator was used as the light source, and the resulting images were analysed with software ImageJ. A MeCN/water (1:1) mixture was used to remain in biologically acceptable environment. A solution of imidazole **3b** was prepared at a concentration of 0.09 mg/mL, despite low fluorescence intensity. This was the achievable concentration maximum due to its limited solubility. Acidic and basic conditions were achieved by adding a minimal amount of aqueous solution of HCl and NaOH. The neutral form was taken as the reference (100%), and changes in fluorescence intensity were measured compared to it. To our surprise, a remarkable increase in fluorescence intensity was observed in the deprotonated form (965%), despite the fact, that the absorbance at the given irradiation wavelength was not very significant (Figures 10–11).

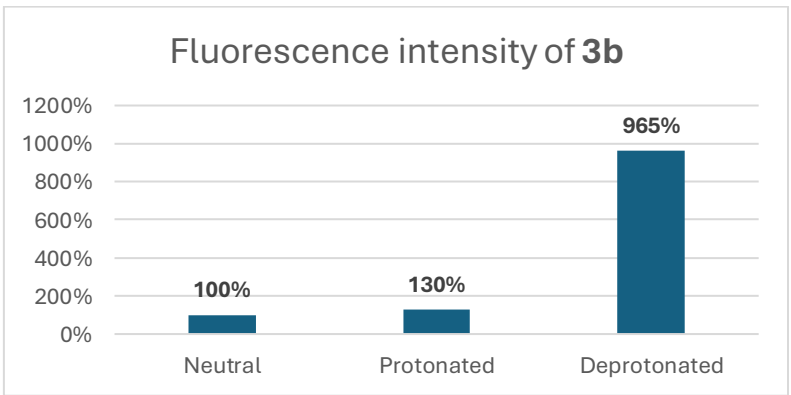

Figure **10** Fluorescence intensity of acid-base forms of **3b**

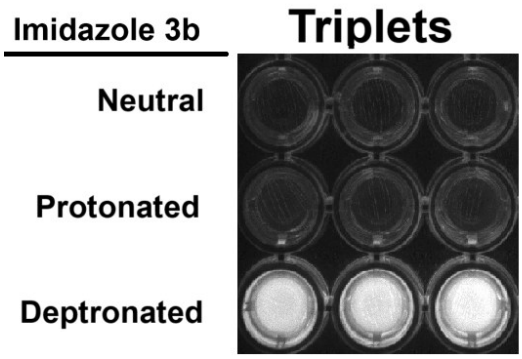

Figure **11** Microtitration plate showing fluorescence intensity based on acid-base form of **3b**

In our imidazole-acridone system, the deprotonated species could form a six-membered pseudo-ring through intramolecular hydrogen bonding (Scheme 23). This interaction could restrict torsional motions, lock the molecular conformation, and reduce non-radiative decay pathways. Such a hydrogen-bond-stabilized ring could also support a more efficient ICT by maintaining a planar alignment between donor and acceptor groups. In turn, this might enhance orbital overlap and promote radiative decay, potentially leading to a higher quantum yield and stronger fluorescence even if the absorbance at the deployed wavelength is lower.

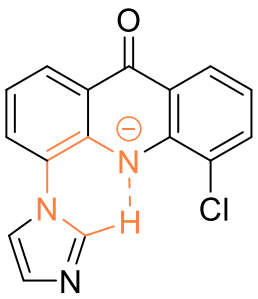

Scheme **23** Proposed explanation of enhanced fluorescence of deprotonated **3b**

4.4. N-alkylation of imidazole ring

4.4.1. Synthesis

Imidazolium salts **4a** and **4b** were synthesized by performing N-alkylation of the imidazole ring with the appropriate alkyl halide, without using solvent. We expected that such a modification could increase the solubility of the compound. The mixture was stirred and heated overnight (Scheme 24).

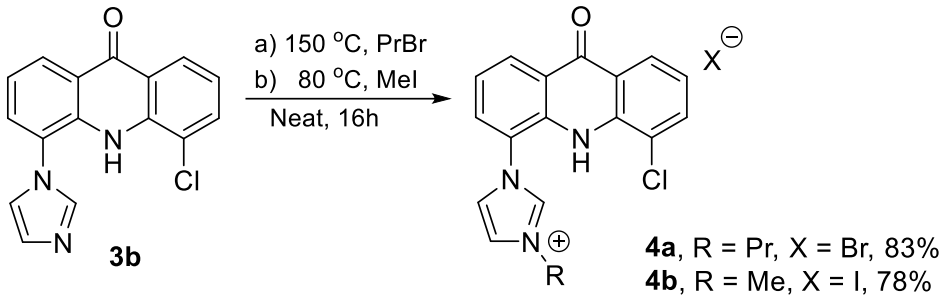

Scheme **24** Synthesis of **4a** and **4b**

a) 4a

Excess bromopropane was used not only as the alkylating agent but also as the reaction medium. The reaction was carried out in a sealed pressure vial, for bromopropane has boiling point of 71 °C. The conversion could be monitored by TLC. No side products were detected in the reaction. The product was further purified by column chromatography to remove small traces of residual starting material. Reaction time of 3 hours resulted in yield of 64% and 16 hours yielded 83%.

b) 4b

This reaction was analogous, apart for a few modifications. A lower temperature of 80 °C was used, as iodomethane has a boiling point of only 43 °C. To remove the excess iodomethane, the crude mixture was loaded onto a chromatographic column and firstly washed with DCM. The product, being highly polar, remained during this step at the top of the column. Subsequently, the mobile phase was changed to a more polar one and the product was purified to eliminate small traces of reactant. A reaction time of 16 hours gave a yield of 78%.

4.4.2. Acid-base and optical properties of 4a

Similarly to **3b**, we attempted to measure the ^{1}H NMR spectrum of **4a** under basic conditions. We expected the enaminone NH signal to disappear, indicating the formation of a zwitterionic form. However, the results showed that in a basic environment, **4a** converted into a different compound, which so far remains unidentified . Furthermore, acidification did not restore the original structure, suggesting that the transformation was irreversible.

We then proceeded with UV-Vis spectroscopy. UV-Vis spectra of imidazolium **4a** were measured in its cationic form and under basic conditions (Figures 12–13). The absorbance maximum for the cationic form was 338.98 nm, while the spectrum under basic conditions showed weaker bands at 331.18 nm and 346.66 nm, along with more distinct peaks at 431.25 nm and 456.62 nm.

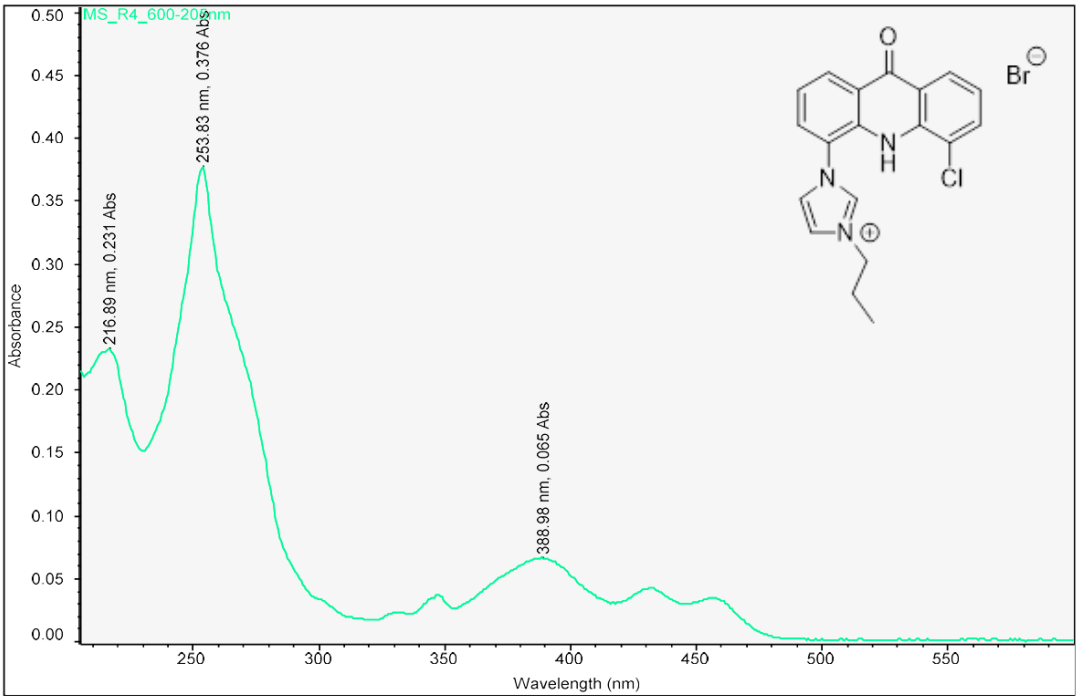

Figure **12** UV-Vis absorption spectrum of **the cationic form of 4a**

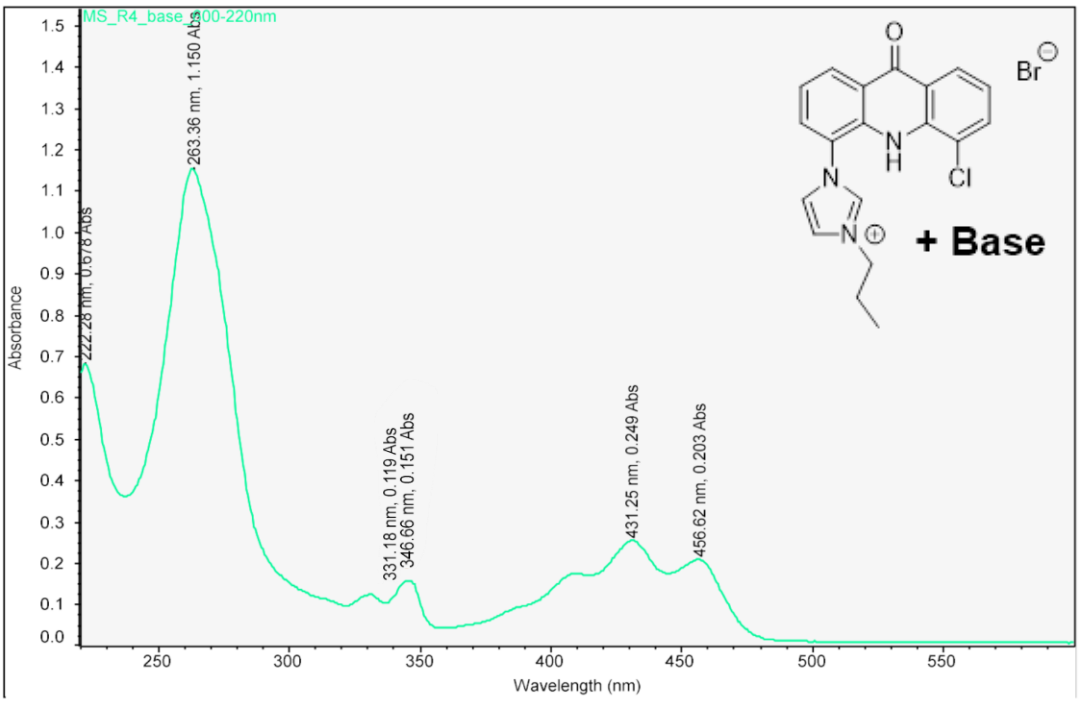

Figure **13** UV-Vis absorption spectrum of the **unspecified base-induced form of 4a**

The same method for measuring intensity was used as for compound **3b.** A MeCN/water (1:1) mixture continued to be used as solvent. Imidazolium displays better solubility than acridone, therefore working concentration was chosen by testing concentrations, ranging from 0.1 mg/mL down to 0.0125 mg/mL. A working concentration of 0.05 mg/mL (0.24 µmol/mL) was selected. The cationic form was taken as the reference (100%), and changes in fluorescence intensity were measured compared to it. A substantial increase was observed in the unspecified base-induced form (234%). (Figures 14–15).

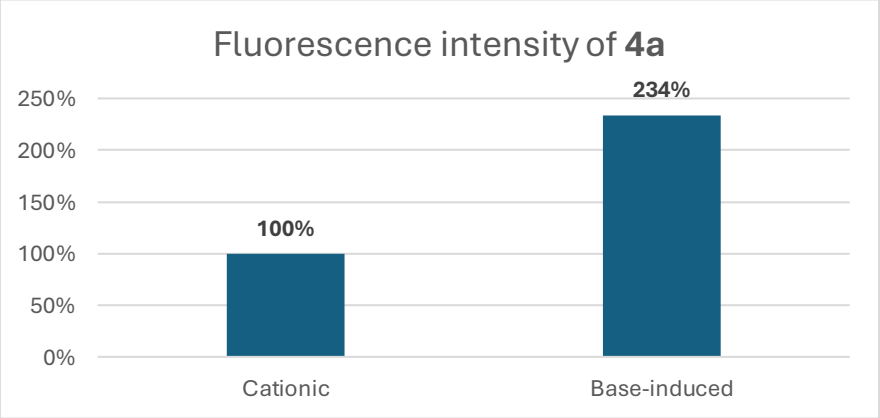

Figure **14** Fluorescence intensity of the cationic and unspecified base-induced form of **4a**

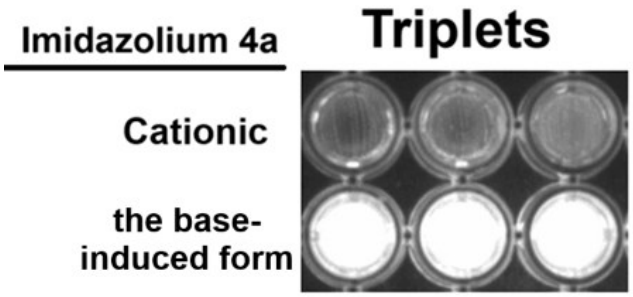

Figure **15** Microtitration plate showing fluorescence intensity of the cationic and unspecified base-induced form of **4a**

4.4.3. Fluorescence response to the presence of metallic salts

As our next goal, we conducted examination of the imidazolium salt **4a** for changes in fluorescence intensity in the presence of metal ions, including various oxidation states. We chose to conduct this testing with only **4a** because the imidazole **3b** exhibited limited solubility in all solvents and we did not manage to work with **4b** due to time constraints.

We followed previously established conditions, using the same measurement method and maintaining the same concentration (0.05 mg/mL) and solvent (MeCN/water, 1:1). DMSO was briefly tested as a solvent; however, it was excluded from further experiments due to a photochemical reaction that caused fluorescence to fade within 10 minutes, due to an unspecific decomposition of the probe. ^{1}H NMR was performed to help identify the formed compound, but we were unable to interpret the results or determine the cause of the decomposition.

To test the change due to a presence of metal, various salts and complexes were added to the compound in a 1:1 molar ratio. The change in intensity was measured relatively to a 0.05 mg/mL solution of our compound, which was set at 100%.

It is important to note that the anions and ligands of the metal salt play a significant role in the outcome. Anions that significantly shift the pH or cause oxidation or reduction were deliberately avoided. However, some potentially interesting metal salts could not be tested due to their limited solubility in the used MeCN/water mixture.

All 28 tested salts and complexes, along with their influence on fluorescence intensity, are shown in (Figure 16). We included biologically relevant metals such as alkali metals, copper, cobalt, and iron, as well as noble and transition metals like cerium, rhodium, ruthenium, platinum, and palladium, in all possible or available oxidation states.

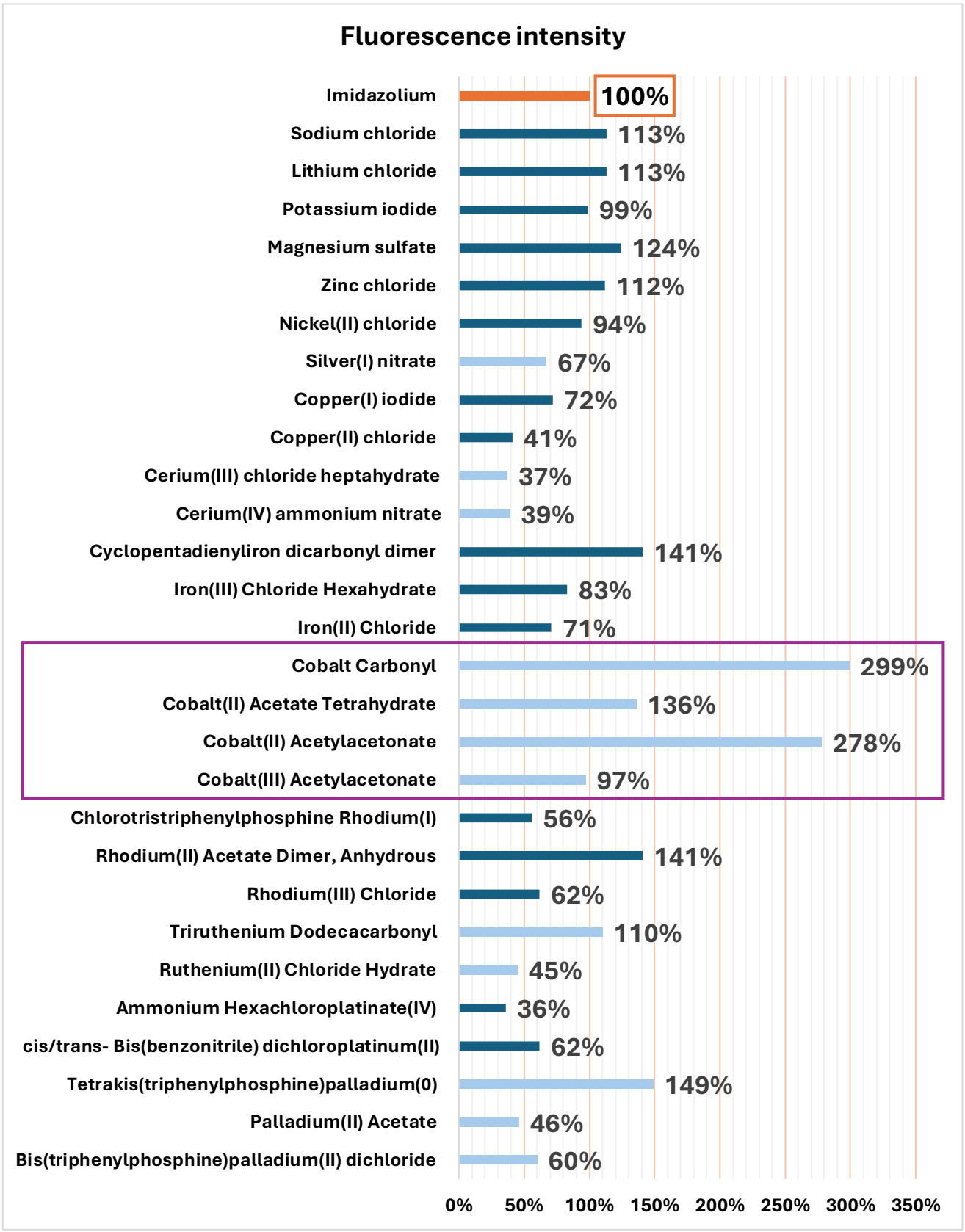

Figure **16** Change in fluorescence intensity of **4a** in presence of various metals salts and complexes

Most tested metals did not produce the desired fluorescence response, as either the signal change was small, making it difficult to distinguish from potential measurement errors, or there was no distinct variation between oxidation states. Some oxidation states are also not exactly stable, example being Fe^{+1} in cyclopentadienyliron dicarbonyl dimer, therefore the results would not be exactly applicable. Precious catalytic metals showed promise, as fluorescence typically changed in their presence. However, the results are not definitive, as these metals were all in different complexes with varying ligands. Only cobalt, among the tested metals, yielded the most promising and definitive results, as Co^{2+} and Co^{3+} were tested using the same counterion. Cobalt(II) acetylacetonate showed increase in fluorescence intensity (278%) as opposed to Cobalt(III) acetylacetonate which led to practically no change (97%), highlighting a clear difference based on oxidation state (Figure 17). Such system seems to be suitable for selective rewritable molecular data storage with potential as a data input (to induce a change in oxidation state of cobalt), and fluorescence as the readout.

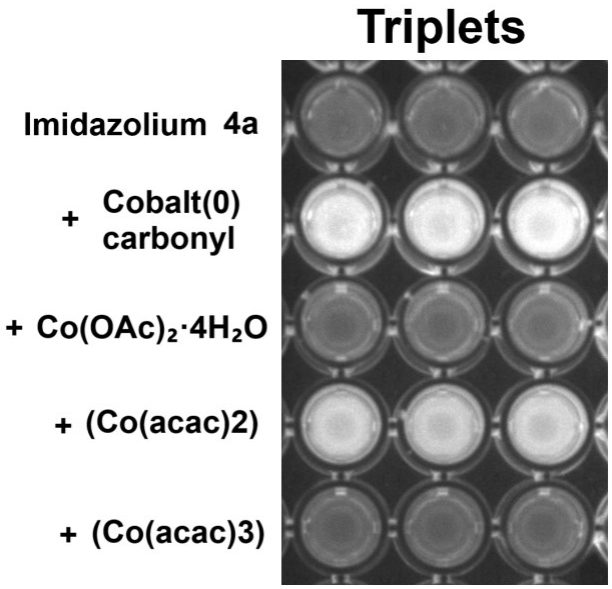

Figure **17** Microtitration plate showing fluorescence change in **4a** in presence of various cobalt salts

5. Experimental part

5.1. Used chemicals

All chemicals used were purchased from OrgChem, Sigma–Aldrich, Fluorochem, Acros Organics, PENTA Chemicals, Alfa Aesar, BLDpharm, Strem Chemicals, Tokyo Chemical Industry, and Lach:ner.

5.2. Used instruments

For TLC analysis, a UV lamp with wavelengths of 254 nm and 365 nm, and TLC plates with F254 bare silica from Silicycle were used. For preparative TLC, glass-backed TLC plates with 60A F254 silica gel from Silicycle were employed. For column chromatography, silica gel 60A (0.040–0.063 mm) was used. All NMR spectra were measured on Bruker Avance III and Bruker Avance NEO 400 MHz spectrometers (400 MHz for ^{1}H and 100 MHz for ^{13}C) and Bruker Avance III 600 MHz spectrometer (600 MHz for ^{1}H and 150 MHz for ^{13}C). MS were obtained on a VG-Analytical ZAB SEQ spectrometer. Melting points were measured on a Kofler apparatus (KB T300). IR spectra in the KBr mixture were measured on a Thermo Scientific Nicolet AVATAR 370 FT-IR spectrometer. UV-Vis spectra were measured with Thermo Scientific Helios γ with wolfram and deuterium lamp, wavelength range 190-800 nm. Fluorescence intensity was visualised with the Syngene T-Genius longwave transilluminator with the GeneSys control system. Fluorescence intensity was measured with ImageJ software.

5.3. Use of artificial intelligence

Artificial intelligence (ChatGPT, OpenAI) was employed as a supplementary tool during the preparation of this thesis. It was used to assist with linguistic corrections, offer stylistic improvements, enhance clarity, and eliminate redundancy. All AI-generated content was carefully reviewed, edited, and adapted by the author to ensure accuracy and adherence to academic standards. The use of AI aligns with ethical guidelines and did not replace the author's critical analysis or independent research.

5.4. Synthesis of compounds

5.4.1. 2-[(2-aminophenyl)amino]benzoic acid

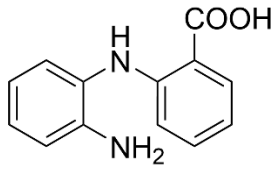

1

2-Chlorobenzoic acid (1.00 g; 6.39 mmol; 1.0 eq), 2-phenylenediamine (0.7239 g; 6.45 mmol; 1.01 eq), potassium carbonate (1.33 g), and copper powder (0.243 g) were combined in DMF (25 mL) and stirred under an inert atmosphere at 170 °C for 16 hours. After completion, the reaction mixture was filtered through filter paper to remove solids, yielding a filtrate containing the product. DMF was removed from the filtrate via vacuum distillation (10 mbar) while maintaining a vapor temperature of 40–48 °C. The reaction mixture was subjected to column chromatography, using silica gel as the stationary phase. Hexane was first used as the mobile phase to remove any remaining DMF. The column was deactivated with TEA. Following this, a DCM/MeOH mobile phase was used, starting with a 50:1 ratio, with gradual adjustment to 10:1 ratio. Compound **1** was obtained as a red amorphous solid in 17% yield (245 mg).

R_f (DCM/MeOH 50:1) = 0.81

M.p. 198 – 205 °C.

^{1}H NMR (400 MHz, DMSO) δ 9.04 (s, 1H), 7.85 (dd, *J* = 8.0, 1.7 Hz, 1H), 7.28 (ddd, *J* = 8.7, 7.0, 1.7 Hz, 1H), 7.03 (dd, *J* = 7.8, 1.5 Hz, 1H), 6.96 (td, *J* = 7.6, 1.5 Hz, 1H), 6.80 (dd, *J* = 8.1, 1.4 Hz, 1H), 6.65 (t, *J* = 7.5 Hz, 1H), 6.62 – 6.54 (m, 2H). 4,85 (s, 2H). Due to water in DMSO carboxylic proton is not seen.

^{13}C NMR (101 MHz, DMSO) δ 170.1, 149.2, 144.2, 134.0, 131.6, 126.3, 126.1, 124.8, 116.6, 115.88, 115.4, 113.2, 111.4.

The measured values align with those reported in the literature[45].

5.4.2. 4-aminoacridin-9(10H)-one

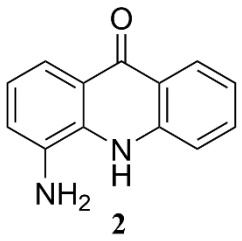

2

To compound **1** (74 mg) was added polyphosphoric acid (1 spoon) and the reaction mixture was stirred at 120 °C for 2.5 h. The mixture was cooled and poured into a flask containing cold water (100 mL) in an ice bath. The resulting aqueous solution was neutralized with KOH to pH 7. The dark yellow precipitate was filtered on a Buchner funnel and washed with water and petroleum ether. Compound **2a** in the appearance of an amorphous yellow solid was prepared in 90% yield (61,3 mg).

R_f (DCM/MeOH 15:1) = 0.63

M.p. 345 °C.

^{1}H NMR (400 MHz, DMSO) δ 10.64 (s, 1H), 8.20 (dd, *J* = 8.1, 1.0 Hz, 1H), 7.70 (dd, *J* = 6.7, 1.6 Hz, 1H), 7.67 – 7.63 (m, 1H), 7.58 – 7.49 (m, 1H), 7.23 (ddd, *J* = 8.1, 6.7, 1.3 Hz, 1H), 7.06 – 6.98 (m, 2H), 5.55 (s, 2H).

^{13}C NMR (101 MHz, DMSO) δ 177.0, 140.6, 136.9, 133.03, 129.7, 125.9, 121.5, 121.5, 120.9, 120.0, 117.6, 115.9, 113.5.

The measured values align with those reported in the literature[45].

5.4.3. 4-chloro-5-(1H-imidazol-1-yl)acridin-9(10H)-one

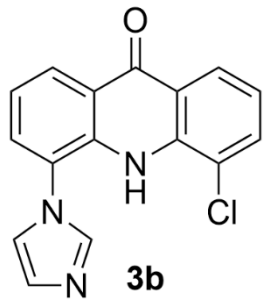

3b

Aminoacridone **2b** (567 mg; 2.32 mmol; 1,0 eq.) was treated with 40% aqueous glyoxal (0,34 mL; 1.2 eq.) in MeOH (20 mL) overnight at room temperature. Subsequently, additional methanol (5 mL), NH_4Br (460 mg, 2 eq.) and paraformaldehyde were added (140 mg; 2 eq.). The mixture was heated under reflux for 1h. Following this, 85% H_3PO_4 (2 mL) was added, and the mixture was stirred under reflux overnight. Upon completion, the mixture was filtered, and the solvent was removed from filtrate under vacuum. The remaining oily filtrate was diluted with water (10 mL) and the mixture was neutralised to pH 7 with 6 M solution of KOH. The formed precipitated crude product was collected by vacuum filtration. Following, the crude product was purified by column chromatography, using silica gel as the stationary phase and DCM/MeOH (50:1) as mobile phase. Compound **3b** was isolated as an orange amorphous solid in 20% yield (142 mg).

R_f (DCM/MeOH 50:1) = 0.70

^{1}H NMR (400 MHz, DMSO) δ 8.69 (bs, 1H), 8.36 (d, *J* = 8.1 Hz, 1H), 8.24 (dd, *J* = 8.1, 1.4 Hz, 1H), 8.14 (bs, 1H), 7.99 (d, *J* = 7.8 Hz, 1H), 7.92 (d, *J* = 7.5 Hz, 1H), 7.83 (bs, 1H), 7.48 (at, *J* = 7.8 Hz, 1H), 7.40 – 7.33 (m, 2H).

^{13}C NMR (151 MHz, DMSO) δ 176.1, 138.4, 136.2, 135.1, 133.7, 131.4, 130.5, 127.2, 126.6, 125.9, 125.5, 122.5, 122.1, 121.8, 120.7, 120.4.

IR (KBr): 3384, 2952, 2924, 2852, 1618, 1593, 1525, 1246, 1174, 1124, 827, 750 cm^{-1}.

M.p. 279.3 °C.

HRMS (ESI) for $C_{16}H_{10}ClN_3O + H^+$ calculated as 296.0589 and measured as 296.0585.

5.4.4. 1-(5-chloro-9-oxo-9,10-dihydroacridin-4-yl)-3-propyl-1H-imidazol-3-ium bromide

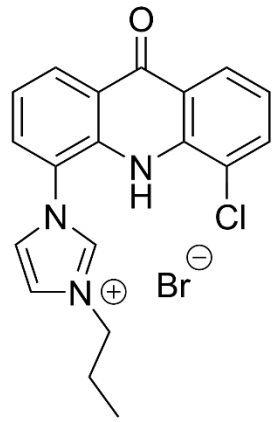

4a

Compound **3b** (100.0 mg; 338 μmol) was treated with bromopropane (2.00 mL) in a pressure vial at 150 °C for 16 hours. The reaction progress was monitored by TLC (DCM/MeOH, 20:1). Upon complete conversion of reactants, excess bromopropane was removed under reduced pressure. The crude product was purified by column chromatography, using silica gel as the stationary phase and DCM/MeOH (20:1 → 5:1) as mobile phase. Compound **4a** was obtained as a brown amorphous solid in 83% yield (117 mg).

R_f (DCM/MeOH 15:1) = 0.26

^{1}H NMR (400 MHz, DMSO) δ 9.88 (s, 1H), 9.75 (s, 1H), 8.47 (d, *J* = 8.0 Hz, 1H), 8.35 (bs, 1H), 8.26 (d, *J* = 8.0 Hz, 1H), 8.17 (bs, 1H), 8.13 (d, *J* = 7.4 Hz, 1H), 8.01 (d, *J* = 7.4 Hz, 1H), 7.56 (at, *J* = 8.0 Hz, 1H), 7.38 (at, *J* = 8.0 Hz, 1H), 4.31 (t, *J* = 7.1 Hz, 2H), 1.99 (m, 2H), 1.02 (t, *J* = 7.3 Hz, 3H).

^{13}C NMR (101 MHz, DMSO) δ 176.0, 138.5, 136.9, 135.1, 134.3, 132.4, 128.6, 125.5, 123.9, 123.4, 123.2, 122.9, 122.4, 122.3, 122.1, 121.4, 50.9, 22.8, 10.7.

IR (KBr): 3396, 3126, 3037, 2962, 2925, 2852, 1620, 1599, 1549, 1523, 1252, 1205, 1173, 1105, 791, 750 cm^{-1}.

M.p. 264.3 °C.

HRMS (ESI$^+$) for $C_{19}H_{17}ClN_3O^+$ was calculated as 338.1087 and measured as 338.1056.

5.4.5. 1-(5-chloro-9-oxo-9,10-dihydroacridin-4-yl)-3-methyl-1H-imidazol-3-ium iodide

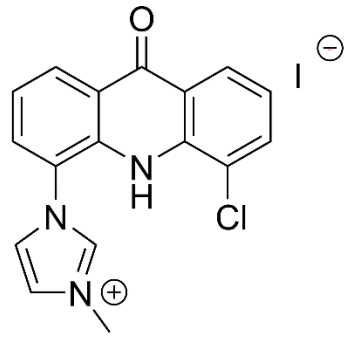

4b

Compound **3b** (16.0 mg; 54 μmol) was treated with methyl iodide (0.5 mL) in a pressure vial at 80 °C for 16 hours. Afterwards, the reaction mixture was transferred onto chromatography column, using silica gel as the stationary phase, where it was washed with DCM to remove MeI. Afterwards, the mobile phase was changed to DCM/MeOH (20:1 → 5:1) and the crude product was purified. Compound **4b** was obtained as a brown amorphous solid in 78% yield (18.5 mg).

R_f (DCM/MeOH 8:1) = 0.21

^{1}H NMR (400 MHz, DMSO) δ 9.74 (s, 1H), 9.69 (s, 1H), 8.47 (d, *J* = 8.0 Hz, 1H), 8.31 (s, 1H), 8.25 (d, *J* = 7.9 Hz, 1H), 8.09 (d, *J* = 7.4 Hz, 1H), 8.06 (bs, 1H), 8.00 (d, *J* = 7.4 Hz, 1H), 7.55 (at, *J* = 8.0 Hz, 1H), 7.38 (at, *J* = 7.9 Hz, 1H), 4.03 (s, 3H).

^{13}C NMR (151 MHz, DMSO) δ 176.0, 139.4, 136.9, 135.2, 134.4, 132.4, 128.7, 125.5, 124.4, 123.8, 123.0, 123.0, 122.4, 122.3, 122.1, 121.4, 36.1.

IR (KBr): 3438, 3390, 2962, 2924, 2850, 1732, 1635, 1547, 1385, 1350, 1261, 1233, 1097, 1049, 754, 727 cm^{-1}.

M.p.: compound carbonised before melting.

HRMS (ESI$^+$) for $C_{17}H_{13}ClN_3O^+$ was calculated as 310.0742 and measured as 310.0740.

6. Conclusion and outlook

Despite some initial challenges with low yields in our synthetic plan, which led us to switch to an another derivate, we successfully synthesized the imidazole-acridone compound **3b** and its corresponding imidazolium salts, propylated **4a** and methylated **4b**. This allowed us to establish a reliable synthetic route to highly fluorescent and structurally versatile molecules. While **3b** and **4a** were further studied as fluorescent probes, compound **4b** was not tested for its acid-base or optical properties due to time constraints; however, its similar structure holds potential for future investigation.

Fluorescence studies of **3b** across acidic and basic conditions revealed an exceptional increase of fluorescence intensity (965%) in its deprotonated form. Compound **3b** also exhibited reversible fluorescence response. Similarly, the imidazolium salt **4a** exhibited an increase in fluorescence (234%) in its unspecified form that is present under basic conditions. Future studies could explore more gradual pH shifts (such as through fluorescent titration) to better understand the pH-dependent changes in fluorescence, as only extreme pH conditions were tested here.

Moreover, compound **4a** was tested for fluorescence response in the presence of various metal ions in varying oxidation states. While it did not show selectivity for typical biogenic metals, a notable response was observed for cobalt. Changes in intensity for different oxidation states were also shown in the presence of precious catalytic metals like palladium.
The ability of **4a** to modulate its fluorescence response based on pH conditions and selective cobalt sensing highlights its potential as a dual fluorescent probe. The pH response, combined with our ability to control the cobalt oxidation state through the modulation of an electrochemical potential, makes it well-suited as a molecular switch with potential applications in data storage systems.

These results lay the foundation for future studies on the structure–property relationships of imidazole acridones. This paves the way for their application in data storage, chemical sensing, and other molecular technologies.

7. Acknowledgements

I would like to sincerely thank my supervisor, Dr. Lukáš Rýček, M.Sc., for his exceptional guidance, continuous support, and patience throughout my research journey. I also want to extend my gratitude to my lab members, Mgr. Dominik Kunák, Bc. Tereza Havlíková, and Dr. Miguel Mateus, M.Sc., for their help and support. Finally, I am deeply thankful to my family and friends for their constant encouragement and support.

8. Literature

(1) Nandi, S.; Bhunia, S.; Debnath, I.; Hazra, S.; Ghosh, S.; Hazra, S. Different Biological Activities and Structure Activity Studies of Acridine and Acridone Derivatives: An Updated Review. *World J. Pharm. Res.* **2024**, *13* (16), 357–399.

(2) Vaddamanu, M.; Sathyanarayana, A.; Masaya, Y.; Sugiyama, S.; Kazuhisa, O.; Velappan, K.; Nandeshwar, M.; Hisano, K.; Tsutsumi, O.; Prabusankar, G. Acridine N-Heterocyclic Carbene Gold(I) Compounds: Tuning from Yellow to Blue Luminescence. *Chem. – Asian J.* **2021**, *16* (5), 521–529. https://doi.org/10.1002/asia.202001380.

(3) Kumar, R.; Sharma, S.; Prasad, D. Chapter 3 - Acridones: A Relatively Lesser Explored Heterocycle for Multifactorial Diseases. In *Key Heterocycle Cores for Designing Multitargeting Molecules*; Silakari, O., Ed.; Elsevier, 2018; pp 53–132. https://doi.org/10.1016/B978-0-08-102083-8.00003-0.

(4) Drechsler, K. Über Eine Bei Der Einwirkung von Aluminiumchlorid Aufo-Nitrobenzylchlorid Und Benzol Entstehende Base C13 H9 NO. *Monatshefte Für Chem. Verwandte Teile Anderer Wiss.* **1914**, *35* (5), 533–560. https://doi.org/10.1007/BF01519382.

(5) Atangana, A. F.; Toze, F. A. A.; Langat, M. K.; Happi, E. N.; Mbaze, L. L. M.; Mulholland, D. A.; Waffo, A. F. K.; Sewald, N.; Wansi, J. D. Acridone Alkaloids from Vepris Verdoorniana (Excell & Mendonça) Mziray (Rutaceae). *Phytochem. Lett.* **2017**, *19*, 191–195. https://doi.org/10.1016/j.phytol.2017.01.001.

(6) Goni, L. K. M. O.; Jafar Mazumder, M. A.; Tripathy, D. B.; Quraishi, M. A. Acridine and Its Derivatives: Synthesis, Biological, and Anticorrosion Properties. *Materials* **2022**, *15* (21). https://doi.org/10.3390/ma15217560.

(7) Om Silakari. *Key Heterocycle Cores for Designing Multitargeting Molecules*, 1st Edition.; Elsevier, 2018.

(8) Kumar, R.; Kumari, M. Chemistry of Acridone and Its Analogues: A Review. *J. Chem. Pharm. Res.* **2011**, *3*, 217–230.

(9) Horne, S.; Rodrigo, R. A Short Efficient Route to Acronycine and Other Acridones. *J. Chem. Soc. Chem. Commun.* **1991**, No. 15, 1046–1048. https://doi.org/10.1039/C39910001046.

(10) Waterman, P. G. Alkaloids of the Rutaceae: Their Distribution and Systematic Significance. *Biochem. Syst. Ecol.* **1975**, *3* (3), 149–180. https://doi.org/10.1016/0305-1978(75)90019-8.

(11) Prasher, P.; Sharma, M. Medicinal Chemistry of Acridine and Its Analogues. *MedChemComm* **2018**, *9* (10), 1589–1618. https://doi.org/10.1039/C8MD00384J.

(12) Piboonprai, K.; Khumkhrong, P.; Khongkow, M.; Yata, T.; Ruangrungsi, N.; Chansriniyom, C.; Iempridee, T. Anticancer Activity of Arborinine from Glycosmis Parva Leaf Extract in Human Cervical Cancer Cells. *Biochem. Biophys. Res. Commun.* **2018**, *500* (4), 866–872. https://doi.org/10.1016/j.bbrc.2018.04.175.

(13) Wang, C., Wan, J., Mei, Z., & Yang, X. Acridone Alkaloids with Cytotoxic and Antimalarial Activities from Zanthoxylum Simullans Hance. *Pharmacogn. Mag.* **2014**, *10(37)*, 73–76. https://doi.org/doi: 10.4103/0973-1296.126669.

(14) Nguyen, Q. C.; Nguyen, T. T.; Yougnia, R.; Gaslonde, T.; Dufat, H.; Michel, S.; Tillequin, F. Acronycine Derivatives: A Promising Series of Anticancer Agents. *Anticancer Agents Med Chem* **2009**, *9* (7), 804–815. https://doi.org/10.2174/187152009789056921.

(15) Liu, C.; Li, S. Engineered Biosynthesis of Plant Polyketides by Type III Polyketide Synthases in Microorganisms. *Front. Bioeng. Biotechnol.* **2022**, *Volume 10-2022*. https://doi.org/10.3389/fbioe.2022.1017190.

(16) IUBMB. Acridone. International Union of Biochemistry and Molecular Biology, Queen Mary University of London. *Acridone Alkaloid Biosynthesis*. https://iubmb.qmul.ac.uk/enzyme/reaction/alkaloid/acridone.html (accessed 2025-04-30).
(17) Gogoi, U.; Pathak, K.; Saikia, R.; Pathak, M. P.; Paul, T.; Khan, S. A.; Das, A. Recent Advances on Natural and Non-Natural Xanthones as Potential Anticancer Agents: A Review. *Med Chem* **2023**, *19* (8), 757–784. https://doi.org/10.2174/1573406419666221226093311.
(18) Marques, T. J. S.; Salvador, D.; Oliveira, H.; Serra, V. V.; Paradis, N.; Wu, C.; Silva, V. L. M.; Ramos, C. I. V. New Acridone Derivatives to Target Telomerase and Oncogenes – an Anticancer Approach. *RSC Med Chem* **2025**. https://doi.org/10.1039/D4MD00959B.
(19) Voura, M.; Khan, P.; Thysiadis, S.; Katsamakas, S.; Queen, A.; Hasan, G. M.; Ali, S.; Sarli, V.; Hassan, Md. I. Probing the Inhibition of Microtubule Affinity Regulating Kinase 4 by N-Substituted Acridones. *Sci. Rep.* **2019**, *9* (1), 1676. https://doi.org/10.1038/s41598-018-38217-8.
(20) Gopinath, V. S.; Thimmaiah, P.; Thimmaiah, K. N. Acridones Circumvent P-Glycoprotein-Associated Multidrug Resistance (MDR) in Cancer Cells. *Nucleic Acid Modif. Fluroescence-Based Technol.* **2008**, *16* (1), 474–487. https://doi.org/10.1016/j.bmc.2007.09.020.
(21) Sulthanudeen, S.; Imran, P. M.; Selvakumaran, M.; Kubaib, A. Novel Acridone Derivatives Probed Using DFT, Including Design, Synthesis, Characterization with Anti-Oxidant and Anti-Mitotic Screening. *Results Chem.* **2023**, *5*, 100753. https://doi.org/10.1016/j.rechem.2022.100753.
(22) Mehta, G.; Sambaiah, T.; Maiya, B. G.; Sirish, M.; Chatterjee, D. Synthesis and Nuclease Activity of Some 'Porphyrin–Acridone' Hybrid Molecules. *J. Chem. Soc. Perkin 1* **1993**, No. 22, 2667–2669. https://doi.org/10.1039/P19930002667.
(23) *Acridine Orange: A Review of Novel Applications for Surgical Cancer Imaging and Therapy*.
(24) Lee, H. S.; Guo, J.; Lemke, E. A.; Dimla, R. D.; Schultz, P. G. Genetic Incorporation of a Small, Environmentally Sensitive, Fluorescent Probe into Proteins in Saccharomyces Cerevisiae. *J. Am. Chem. Soc.* **2009**, *131* (36), 12921–12923. https://doi.org/10.1021/ja904896s.
(25) Fu, Y.; Finney, N. S. Small-Molecule Fluorescent Probes and Their Design. *RSC Adv.* **2018**, *8* (51), 29051–29061. https://doi.org/10.1039/C8RA02297F.
(26) Tian, M.; Ma, Y.; Lin, W. Fluorescent Probes for the Visualization of Cell Viability. *Acc. Chem. Res.* **2019**, *52* (8), 2147–2157. https://doi.org/10.1021/acs.accounts.9b00289.
(27) Tsien, R. Y. THE GREEN FLUORESCENT PROTEIN. *Annual Review of Biochemistry*, 1998, *67*, 509–544. https://doi.org/10.1146/annurev.biochem.67.1.509.
(28) Setsukinai, K.; Urano, Y.; Kakinuma, K.; Majima, H. J.; Nagano, T. Development of Novel Fluorescence Probes That Can Reliably Detect Reactive Oxygen Species and Distinguish Specific Species*210. *J. Biol. Chem.* **2003**, *278* (5), 3170–3175. https://doi.org/10.1074/jbc.M209264200.
(29) Zheng, H.; Zhan, X.-Q.; Bian, Q.-N.; Zhang, X.-J. Advances in Modifying Fluorescein and Rhodamine Fluorophores as Fluorescent Chemosensors. *Chem Commun* **2013**, *49* (5), 429–447. https://doi.org/10.1039/C2CC35997A.
(30) Li, X.; Zhang, S.; Cao, J.; Xie, N.; Liu, T.; Yang, B.; He, Q.; Hu, Y. An ICT-Based Fluorescent Switch-on Probe for Hydrogen Sulfide in Living Cells. *Chem Commun* **2013**, *49* (77), 8656–8658. https://doi.org/10.1039/C3CC44539A.

(31) Zhang, X.-F.; Zhang, T.; Shen, S.-L.; Miao, J.-Y.; Zhao, B.-X. A Ratiometric Lysosomal pH Probe Based on the Coumarin–Rhodamine FRET System. *RSC Adv* **2015**, *5* (61), 49115–49121. https://doi.org/10.1039/C5RA06246B.
(32) Xia, Y.; He, W.; Li, J.; Zeng, L.; Chen, T.; Liao, Y.; Sun, W.; Lan, J.; Zhuo, S.; Zhang, J.; Yang, H.; Chen, J. Acridone Derivate Simultaneously Featuring Multiple Functions and Its Applications. *Anal. Chem.* **2019**, *91* (13), 8406–8414. https://doi.org/10.1021/acs.analchem.9b01289.
(33) Chattopadhyay, S. K.; Maitra, R.; Kundu, I.; Jana, M.; Mandal, S. K.; Khuda-Bukhsh, A. R. Acridone–Pterocarpan Conjugate: A Hybrid Molecular Probe for Recognition of Nucleic Acids. *Eur. J. Org. Chem.* **2013**, *2013* (36), 8145–8153. https://doi.org/10.1002/ejoc.201301007.
(34) Qiu, B.; Guo, L.; Chen, Z.; Chi, Y.; Zhang, L.; Chen, G. Synthesis of N-4-Butylamine Acridone and Its Use as Fluorescent Probe for ctDNA. *Sel. Pap. Tenth World Congr. Biosens. Shangai China May 14-16 2008* **2009**, *24* (5), 1281–1285. https://doi.org/10.1016/j.bios.2008.07.055.
(35) Kaur, J.; Singh, P. ATP Selective Acridone Based Fluorescent Probes for Monitoring of Metabolic Events. *Chem Commun* **2011**, *47* (15), 4472–4474. https://doi.org/10.1039/C1CC10253B.
(36) Panfilov, M.; Chernova, D.; Khalfina, I.; Moskalensky, A.; Vorob'ev, A. Design and Synthesis of New Acridone-Based Nitric Oxide Fluorescent Probe. *Molecules* **2021**, *26* (14). https://doi.org/10.3390/molecules26144340.
(37) Huang, C.; Yan, S.-J.; Li, Y.-M.; Huang, R.; Lin, J. Synthesis of Polyhalo Acridones as pH-Sensitive Fluorescence Probes. *Bioorg. Med. Chem. Lett.* **2010**, *20* (15), 4665–4669. https://doi.org/10.1016/j.bmcl.2010.05.101.
(38) Aarjane, M.; Slassi, S.; Amine, A. Novel Highly Selective and Sensitive Fluorescent Sensor for Copper Detection Based on N-Acylhydrazone Acridone Derivative. *J. Mol. Struct.* **2020**, *1199*, 126990. https://doi.org/10.1016/j.molstruc.2019.126990.
(39) Huang, J.; Yan, Z.; Qiu, P.; Mo, Y.; Cao, Q.; Li, Q.; Huo, L.; Zhao, L. A New Coumarin-Acridone Compound as a Fluorescence Probe for Fe3+ and Its Application in Living Cells and Zebrafish. *Molecules* **2021**, *26* (8), 2115. https://doi.org/10.3390/molecules26082115.
(40) Prof. Dr. Ben L. Feringa, Dr. Wesley R. Browne. *Molecular Switches*; Wiley-VCH Verlag GmbH & Co. KGaA, 2011.
(41) Copko, J.; Slanina, T. Multiplicity-Driven Photochromism Controls Three-State Fulgimide Photoswitches. *Chem Commun* **2024**, *60* (28), 3774–3777. https://doi.org/10.1039/D3CC05975H.
(42) Zhang, J. L.; Zhong, J. Q.; Lin, J. D.; Hu, W. P.; Wu, K.; Xu, G. Q.; Wee, A. T. S.; Chen, W. Towards Single Molecule Switches. *Chem Soc Rev* **2015**, *44* (10), 2998–3022. https://doi.org/10.1039/C4CS00377B.
(43) Buskirk, A. R.; Liu, D. R. Creating Small-Molecule-Dependent Switches to Modulate Biological Functions. *Chem. Biol.* **2005**, *12* (2), 151–161. https://doi.org/10.1016/j.chembiol.2004.11.012.
(44) Saxer, S.; Marestin, C.; Mercier, R.; Dupuy, J. The Multicomponent Debus–Radziszewski Reaction in Macromolecular Chemistry. *Polym. Chem.* **2018**, *9* (15), 1927–1933. https://doi.org/10.1039/C8PY00173A.
(45) Tian, L.; Feng, C. J.; Li, T. X.; Li, Z.; Yang, W. H.; Han, X. E. Design, Synthesis, Antitumor Evaluation, 3D-QSAR and Molecular Docking Studies of Novel 4-Aminoacridone Compounds. *Med. Chem. Res.* **2017**, *26* (10), 2538–2546. https://doi.org/10.1007/s00044-017-1953-3.

(46) Wolkenberg, S. E.; Wisnoski, D. D.; Leister, W. H.; Wang, Y.; Zhao, Z.; Lindsley, C. W. Efficient Synthesis of Imidazoles from Aldehydes and 1,2-Diketones Using Microwave Irradiation. *Org. Lett.* **2004**, *6* (9), 1453–1456. https://doi.org/10.1021/ol049682b.
(47) Liu, H.; Chen, Z.; Ma, Y.; Lv, M.; Yin, S.; Shang, F.; Liu, J. Theoretical Study on the Synthesis Efficiency and Yield of Imidazole Derivatives Based on the Glyoxal and Diamine. *Int. J. Quantum Chem.* **2024**, *124* (19), e27476. https://doi.org/10.1002/qua.27476.